crystals

MDPI

*Review*

# Intermolecular Interactions in Functional Crystalline Materials: From Data to Knowledge

**Anna V. Vologzhanina**

A. N. Nesmeyanov Institute of Organoelement Compounds, RAS. 28 Vavilova street, 119991 Moscow, Russia; vologzhanina@mail.ru

Received: 26 August 2019; Accepted: 12 September 2019; Published: 13 September 2019

check for updates

**Abstract:** Intermolecular interactions of organic, inorganic, and organometallic compounds are the key to many composition–structure and structure–property networks. In this review, some of these relations and the tools developed by the Cambridge Crystallographic Data Center (CCDC) to analyze them and design solid forms with desired properties are described. The potential of studies supported by the Cambridge Structural Database (CSD)-Materials tools for investigation of dynamic processes in crystals, for analysis of biologically active, high energy, optical, (electro)conductive, and other functional crystalline materials, and for the prediction of novel solid forms (polymorphs, co-crystals, solvates) are discussed. Besides, some unusual applications, the potential for further development and limitations of the CCDC software are reported.

**Keywords:** cambridge structural database; crystal structures; knowledge-based analysis; intermolecular interactions; structure–property relations; supramolecular chemistry

## 1. Introduction

The history of investigations devoted to the analysis of networks between chemical composition, molecular, and crystal structures and numerous properties of compounds dates back to 1960s. The development of the X-ray diffraction technique and computational routines allowed to collect information about crystal structures of plenty of inorganic, organic, organometallic, and macromolecular compounds. Early findings in the field of composition–structure–properties networks of these solids gave us knowledge about the typical molecular geometry [1,2], steric, and electronic effects of functional groups [3,4], principles of molecular packing [5], role and energetic of numerous intermolecular interactions [6,7]. Longstanding efforts of the crystallographic community to present crystallographic data in a machine-processed format, and to collect these data in crystallographic databases combined with recent progress in software development promotes further insights into the synthesis of novel solids with desired physicochemical properties (including optical, magnetic, electrical, mechanical, and others).

The literature contains numerous review articles devoted to recent advances in crystal engineering [8,9], design of functional organic (see, for example, Refs. [10–13]) and inorganic [14,15] materials, and the development of software for analysis of molecular crystals [16–18]. However, in my opinion knowledge-based analysis and corresponding software are still insufficiently used by chemists, who often analyze relations between functional properties and intermolecular interactions on the level of bond geometry and Figures of crystal packing. On the other hand, analysis of applications of the software by the end users of software can help software developers to find and overcome limitations of their algorithms, and to propose lines for further development. Thus, in the present paper, to demonstrate the effectiveness of knowledge-based analysis of structure–property relations in crystals, some of the relations, possible application of data–knowledge studies, and predictions to analyze them, and a brief description of procedures will be described. Among a huge number of papers published in

these fields, the manuscript cites only (*i*) recent works devoted to the analysis of correlations between intermolecular interactions and properties of a small molecule (for example its inclination to form polymorphs, solvates, and co-crystals), or a corresponding solid (from a well-known requirement for non-linear optical materials to crystallize in acentric space groups, to recent studies devoted to the effect of solvent presence on mechanical properties), and (*ii*) the corresponding software developed to investigate these correlations and to design novel solid forms with desired physicochemical properties. As the description of structure–property networks describes mainly the papers published in the last 10 years in the field of organic, organometallic, and coordination crystals, then the software under discussion will be limited with those developed by the Cambridge Crystallographic Data Centre (CCDC) for material chemistry and crystallography. Various examples of applications of the CCDC software to functional materials including their combination with other software, and restrictions found, will be given.

First, the Cambridge Structural Database (CSD) and components of the CSD-Enterprise will be described in Section 2. Then, some properties related to the appearance of a given supramolecular associate, and the tools to search for an associate in the CSD will be reported in Section 3. The properties of solids dependent on the crystal morphology, the Bravais, Friedel, Donnay, and Harker (BFDH) tool for crystal morphology prediction and its' application to affect crystal morphology, polymorphism, and solvatomorphism will be reported in Section 4. Knowledge-based predictions of H-bonded polymorphism, co-crystal formation, mapping of likely intermolecular interactions, and conformer generation for the synthesis of novel functional materials will be discussed in Section 5, and the analysis of local connectivity and whole architectures of solvent molecules in Section 6. Finally, Section 7 contains information about Python API algorithms compatible with the CSD-Enterprise and about some examples of the successful combination of the CSD-Enterprise tools with external software applicable for investigations in the field of structure–property networks.

## 2. The Cambridge Structural Database (CSD) and its' Libraries and Modules

The Cambridge Structural Database [19,20] is one of several databases containing crystal structures of various compounds whose structures have been determined using crystallographic techniques. Particularly, the CSD contains crystal structures of organic, and organoelement compounds, and metal–organic complexes. These data are collected from publications all other the world combined with structural determinations with no accompanying manuscript. Single-crystal data are included to the CSD even if no coordinates are available, while powder studies are included only if cell parameters, atomic coordinates, and refinement details were reported. The original value of the CSD was to simplify access to individual structures, to help crystallographers to avoid redetermination of previously reported structures, and to allow easy sharing of work within the chemical and crystallographic community. In 2019, the number of the CSD individual entries overpassed 1,000,000! This value can be compared with ca. 200,000 of inorganic crystal structures from the Inorganic Crystal Structures Database (ICSD) [21], or 150,000 entries from the Protein Data Bank (PDB) [22].

The second benefit of the database comes from data–knowledge analysis derived from the entire collection. Since the late 1960s, analysis of crystallographic data allowed us to demonstrate a non-uniform distribution of crystal systems and space groups, to estimate ionic and van-der-Waals radii of various elements, or to propose close packing of molecules within a crystal. Analysis of intermolecular distances to reveal structure-forming interactions has been known for tens of years; the role of hydrogen bonds, π...π stacking, and halogen...halogen interactions can not be overestimated [6,7]. Nowadays, information about the crystal structures of discrete organic and organometallic compounds allows us to reformulate principles of their packing [23,24], and to investigate intermolecular interactions more thoroughly. Not only information about geometry and frequency of occurrence of an unusual interaction, synthon, or tecton is extracted from the CSD to support a conclusion about its' role in crystal packing and electronic effects that cause its' appearance [25–29]; but it is also recommended to additionally compare interaction occurrence relative to what would be expected at random [30–33].

Data about molecular geometry—from bond lengths and angles to torsions and ring geometry—form the basis of our understanding of the energetics of molecular conformation. Analysis of these data allows us to understand not only the most stable conformations, but also to rationalize steric and electronic effects of substitutents, or co-formers on the geometry, or to link it with a reaction pathway [34–36].

Taking the value of the conformational preferences exhibited by molecular fragments, and intermolecular interactions into account, two dynamic knowledge-based libraries were derived from the CSD. These are: *Mogul* [37], which stores intramolecular information, and *IsoStar* [38], which collects information about intermolecular interactions. *Mogul* contains information about millions of bond lengths, angles, and torsions, each relating to a specific chemical environment. Data from this library can be organized into distributions providing a click-of-a-button access to structures used to construct the distribution. Besides, one can check the geometry of a novel structure (this is of importance for structure refinement from powder X-Ray diffraction data, or for understanding the environmental effects of combinative factors and steric exclusion) or to check the geometry of a protein–ligand docking pose. Data for *Isostar* were collected not only from the CSD, but also from protein–ligand complexes in the PDB having a resolution better than 2 Å, and ab initio data of the key interactions. *Isostar* provides the searchable distribution of contact functional groups around a central one (such distributions can be obtained for either the CSD or the PDB collections), and data about geometry (and sometimes energy) of various interactions.

Thus, the CSD and associated libraries serve also as sources of supramolecular knowledge for applications software that addresses specific problems in structural chemistry, rational drug design and crystal engineering. In accord with these tasks, various modules comprising the CSD-Enterprise suite are under constant development (Figure 1). The CSD-System contains the CSD, *Mogul*, and *Isostar* databases; *ConQuest* and *webCSD* provide off-line and on-line searches within the CSD; *Mercury* and *Hermes* are the CCDC's 3D vizualizers of, respectively, small and macromolecular crystal structures. Currently, both *Hermes* and *Mercury* are linked with some CSD-Materials and the CSD-Discovery tools of the CSD-Enterprise. The CSD-Materials module serves for use in crystal engineering and materials design, as well as for the structure solution from powder XRD data with *DASH package*. Various tools and programs for drag analysis and discovery are combined within the CSD-Discovery module. Note, that the *Full Interaction Map* (FIM) tool and *Conformer Generator* tool are intensively used for both material chemistry and drug design. At last, every scientist from this community is welcome to install previously published or to write (and distribute) his/her own CSD Python API scripts.

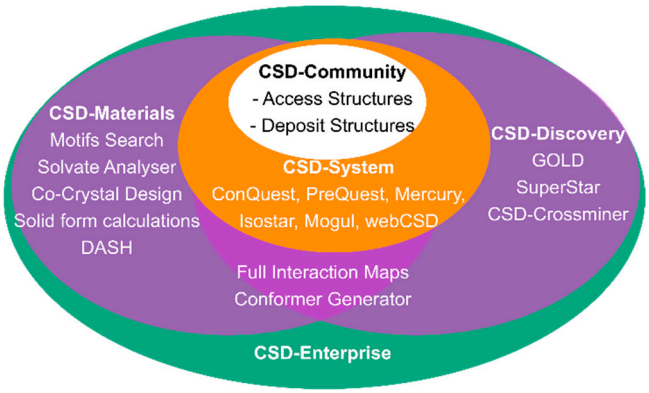


**Figure 1.** Modules comprising the Cambridge Structural Database (CSD)-Enterprise (ver. 2019).

*The CSD-Materials Module*

The main CSD module applicable for investigation and comparison of solid forms and intermolecular interactions, which govern packing of these solids, is the CSD-Materials module. Its' components in the CSD-2019 version allow us to perform:

- Analysis of H-bond motifs (searching of motifs and statistics of their occurrences; assessing the risk of polymorphism via H-bond propensities; prediction of co-crystal formation).
- Analysis of crystal packing features (searching on selected motifs, analysis of packing similarity and building of a packing similarity tree diagram).
- Calculation of theoretical crystal morphology, gas phase MOPAC (Molecular Orbital PACkage) calculation and 'UNI' (UNIversal) force field intermolecular energy calculations.
- Mapping of interaction preferences around an isolated molecule.
- Analysis of solvate and hydrate crystal structures (searching and classification of H-bond motifs, calculation of the volume occupied in a unit cell with solvent molecules, mapping of interaction preferences around them).
- Generation of conformers based on geometrical statistics from the CSD.
- Solution of crystal structures from powder diffraction data using *DASH*.

Although this software was developed and attested mainly for pharmaceutical crystal forms, numerous examples of structure–property networks found for other organic and organometallic compounds with valuable optical, electrochemical, mechanical, and other properties are given below. These studies demonstrate that the possible range of applications of the CSD-materials module can be much expanded, although its application to coordination polymers is less diverse.

## 3. Search and Analysis of Supramolecular Associates

### *3.1. Search on Hydrogen-Bond Motifs*

The utility of big-data analysis of intermolecular interactions extracted from crystallographic databases is based on the fact that the frequency distributions of functional group contacts in the CSD are directly related to the corresponding interaction energies in solution [39]. Analysis of crystal packing in pharmaceuticals, their homologues, polymorphs, co-crystals, and solvates gives one information about preferable synthons that could appear in a binding pocket occupied with this drug (although some weak interactions can be over-, or under-estimated). Data knowledge about typical water associates in crystals of small molecules is important for biochemistry as similar hydrate architectures were found in crystals of inorganic, organic, and macromolecular compounds [40,41].

Among all contacts, H-bonds are the strongest and the most directional interactions that play the dominant role in the crystallization and stability of organic solids, thus their analysis is a central theme of crystal engineering [42–44]. For example, stable H-bonding motifs are used widely to fix olefins in photoreactive positions for [2+2] cycloaddition [45,46]. Analysis of H-bonding is important for understanding proton conductivity [47] and high-temperature ferroelectricity caused by proton tautomerism in polar space groups [48–51]. Reversal of an electric field in the latter solids causes a switch of O-H...O or N-H...N bonds to O...H-O or N...H-N ones accompanied with ketone/enol [48] or neutral/zwitterion [49] isomerisation or imidazole tautomerization [50,51] and the polarity reversal.

Comparison of various H-bonded motifs found between similar functional groups allows one not only to estimate which of them is more stable and abundant to occur but also to shed light on stereoelectronic effects stabilizing various associates [29,52,53]. For example, analysis of 23 phenylglicine amide benzaldimines revealed only five types of H-bonded motifs; the choice of the particular motif depends on the number of H-bonding donors and acceptors, the ease with which the motif is formed, and the possibility of the motif to accommodate additional substituents [54]. The stability of polymorphs of a multifunctional molecule is known to be determined by the energy of an H-bonded motif [55]—that is of importance for drug and food industry, production of high-energy compounds, and dyes and pigments. For these materials the presence of uncommon weak H-bonds in an observed solid form can be indicative of the potential for alternative packing to form another polymorph with stronger interactions [56]. Instead, for high-energy compounds strong H-bonded interactions are disadvantageous as these can prevent molecules from dense packing [57–59]. The appearance of particular H-bonded motifs (spiral chains, bilayers, and others) is characteristic for spontaneous

resolution of racemic and nonracemic mixtures of some chiral compounds [60–62] at crystallizations. Other applications of the analysis of H-bonded associates include salt formation via evaluating synthon competition [63,64], assessing putative structures from crystal structure prediction [65], and analysis of H-bonding in drugs and vitamins [66].

Thus, the search for all representatives of a given H-bonded motif, or for all H-bonded motifs found between some functional groups within the CSD, as well as their classification and statistics of occurrence, become of interest. All these possibilities are realized within the *CSD Motif Search* (Figure 2). A user can select a pre-defined motif from a special library or generate a new motif. To generate a motif, one should sketch a functional group, select the atoms of the functional group which define the contact(s) of the motif, define interatomic distance, and select the type of motif (a ring, an infinite, or a discrete chain) and the number of contacts within the motif. The search can be carried out in the current version of the CSD, in individual refcodes and families of refcodes or in files of structures. The results can be viewed by motifs with the number of hits found and the frequency of occurrence or by structures with the motifs found for each hit. As more than one motif can be found in a crystal structure, their combination can give not only ring and chain motifs but also H-bonded layers and frameworks. Unfortunately, classification of all matches in accord with all non-equivalent H-bonding associates is unavailable in the current version. Besides, the notation used to describe these motifs [67] do not correspond to that recommended to describe underlying nets of crystalline networks and clusters [68–71]. Analysis of H-bonded motifs is part of the *H-bond propensity* tool, the *Co-Crystal Formation* tool, and the *Hydrate Analyzer* described in Sections 5.1, 5.2 and 6, respectively.


**Figure 2.** Flowchart for the *CSD Motif Search*.

### 3.2. StudyingCrystal Packing Features

Besides robust and directed intermolecular interactions, such packing features as π...π stacking, dipole...dipole or halogen, pnicogen, and carbon bonding as well as molecular size-shape regularities can become investigation objects. Some properties of solids are associated with molecular packing instead of intermolecular interactions. These are such properties as luminescent properties of co-crystals of anticrowns with aromatic molecules and hydrocarbons [72–74], electroconductivity of layered donor-acceptor complexes [75,76], optical properties of π-conjugated molecules [77,78], dense packing of high-energetic compounds associated with detonation, and stability properties [59,79]. In this context, it becomes of interest how polytopic molecules or molecules with a lack of limited H-bonding functionalities pack, and which factors govern their packing. A comparison of polymorphs, solvates, and co-crystals of such compounds gives a key for better understanding of these factors. For example, an analysis of 88 crystal structures containing trimeric perfluoro-ortho-phenylen mercury (TPPM) revealed only four motifs of their packing with Lewis bases, governed mainly by Hg...C and π...π interactions [80]. It was shown that the type of supramolecular motif strongly correlates with the nature of a co-former. Another example of the role of weak interactions is the co-crystallization of diphenyl dichalcogenides $Ph_2E_2$ (E = Se, Te) with diiodotetrafluorobenzene that is incorporated during crystallization between stable tectonic chain $Ph_2E_2$ architectures, which were also found in the crystals of pure $Ph_2E_2$ [81]. The co-crystallization of this molecule can be considered as a replacement of E–E and Te–π(Ph) chalcogen bonds with I–E and I–π(Ph) halogen bonds via insertion of stacks of halogen bond donors between tectons of halogen acceptors. Analysis of intermolecular interactions by

means of the energy framework diagrams revealed that the energies of corresponding chalcogen and halogen bonds were lower than those between the stacks of pure $Ph_2E_2$ and diiodotetrafluorobenzene, and illustrates an approach to binary crystals formed by matching tectons (that can be found with the *Crystal Packing Features* tool).

Analysis of mutual disposition of molecules, in this case, can be carried out with the *Crystal Packing Features* tool of the CSD-Materials module. In contrast with the *CSD Motif Search*, a "packing feature" can be generated only from a displayed structure by selecting the atoms and bonds to define the feature. A search query is constructed without sketching any functional groups and atoms based on selected atoms, bonds, and intermolecular distances. Then the CSD is searched to identify crystal structures that contain a similar mutual disposition of atoms. The hits are automatically overlaid with the original geometry, and root-mean-square distance (RMSD) value is reported as a measure of packing similarity. For example, the binary stacks of TPPM and aromatic molecules can be found in a series of co-crystals with luminescent properties [72]. This motif, one of four typical for TPPM co-crystals [80], can be constructed from a TPPM molecule and two aromatic $C_6$ rings situated above and below the TPPM meanplane (Figure 3a). The *Crystal Packing Feature* search allows us to extract from the CSD other examples of such potentially luminescent co-crystals, and to compare the distances between the meanplanes of planar molecules as a measure of charge transfer from electron-rich aromatic molecules to anticrowns.

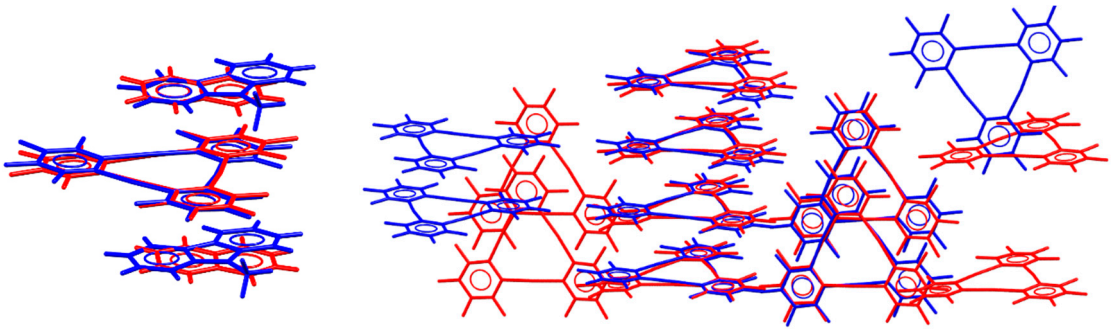

(**a**) (**b**)

**Figure 3.** Examples of the (**a**) *Packing Feature* and (**b**) *Packing Similarity* search hits. A sandwich of a TPPM with two aromatic $C_6$ rings was constructed as the *Packing Feature* from a reference (red) {MOXMIV}[a] molecule and was also found in (blue) {QATTAH}. The *Packing Similarity* comparison of an orthorhombic polymorph of TPPM (blue) {MOXMAN02} with its' three monoclinic polymorphs gives the best similarity with (red) {MOXMAN03}. [a] Here and below a six-letter CSD-Refcode of a compound is given in Figure braces.

A strategy to co-crystal formation based on packing similarity between various co-formers was suggested in Ref. [82]. In this paper, the authors suggested replacing the anion in the crystal of lamaviudine saccharinate with another anion having a similar disposition of acceptor groups (the nature of atoms within acceptors was allowed to vary). Crystal structure and intermolecular interactions of lamaviudine maleate taken as a hit of the CSD search, indeed, were very similar to that of saccharinate. This tool can also be applied to intramolecular interactions or mutial disposition of more than two molecules. For example, the analysis of semicarbazone conformations distinguished that the syn–anti–syn–syn conformation predominates the syn–anti–anti–anti one [83].

### *3.3. Crystal Packing Similarity Tool*

While the *Crystal Packing Features* described above allows one to select from the CSD all supramolecular associates with a user defined mutual disposition of molecules, the *Crystal Packing Similarity* tool can be used to compare a large set of solids containing one co-former and to measure similarity between them, as well as to obtain similarly overlaid molecular packing automatically. This

tool was used for comparison of the experimental crystal structures with those predicted during the sixth blind test of organic crystal structure prediction methods [84]. Such investigations are also of great importance for the analysis of isostructural compounds [85] and some properties that occur only within a given group of supramolecular associates. For example, tetraphenylborates of *N*-salicylideneanilines form isostructural series of photochromic solids due to the packing of cations within a cavity formed by phenyl groups of anions, while more dense packing in other salts gives non-photochromic solids [86]. The effect of substituents on isostructurality of compounds was widely analyzed for both rigid [87–92] and flexible molecules [93–98]. Not only long-accepted isostructurality of Cl- and Me- or -Cl, -Br, and -I substituted molecules were revealed, but also the equivalence of ethylene and azo-bridges [92], or that of azide and iodide substituents [85] were demonstrated. Besides the *Crystal Packing Similarity* tool, XPac [99] and Crycom [100] are also among the software appropriate to carry out such a comparison.

The *Crystal Packing Similarity tool* is applicable to compare multiple structures containing the same compound, e.g., its polymorphs, hydrates, solvates, co-crystals, and salts. Within this method molecular clusters (typically containing a central molecule and its' 14 closest neighbors) are built for each structure, and the clusters are compared with some geometric tolerance to define whether packing is similar or not. Small differences in packings (variation of halogen atoms, absence of some hydrogen atoms, presence of few independent molecules and small co-formers) can be ignored. The results of the comparison are grouped in accord with the number of neighbors forming molecular clusters (from 1 to 2 for different structures to all 14 for pseudo-isostructural compounds), and the groups can also be compared with each other to reveal synthons and associates common for different groups. Such grouping reflects the fact that similar motifs found in polymorphs and solvates typically keep similar intermolecular connectivity and energy of pair interactions [80,101]. The result of such analysis is the dendrogram visualizing crystal packing similarity between different groups of crystal structures. For example, analysis of 50 crystal structures, containing carbamazepin revealed three main motifs ("translation stacks", "inversion cup", and "co-former pairing", Figure 4), and none of these appears via H-bonding [102]. Instead, these motifs seem to represent the most efficient methods for packing of carbamazepin molecules while leaving the carboxamide group free to form hydrogen bonds. Note, that these results coincide with those obtained for carbamazepin-containing solids using the XPac method [103].One of the carbamazepin pseudo-isostructural groups is represented by metastable polymorph II and its solvates and hydrates situated inside the channels formed by the hydrophobic aromatic surfaces of this molecule, which were found to act as stabilizers of this solid [104]. These solvent molecules within the channels can even be replaced with hydrophobic polymer guest molecules [105].

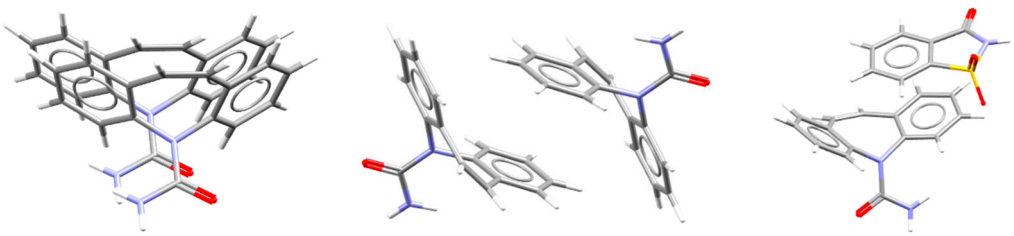

(**a**) (**b**) (**c**)

**Figure 4.** Carbamazepin molecules packed in (**a**) "translation stacks" in {CBMZPN11}, (**b**) "inversion cups" in {CBMZPN01} and (**c**) "co-former pairs" in {UNEZAO}.

Comparison of an orthorhombic polymorph of trimeric perfluoro-ortho-phenylen mercury with its' three monoclinic polymorphs gives up to six similarly packed molecules. Figure 3b visualizes that in crystals of {MOXMAN02} and {MOXMAN03} perfluoro-ortho-phenylen mercury form similar stacks, but these stacks are packed in different ways. The interplay of packing motifs and hydrogen bonds were demonstrated on the example of 37 enantiopure and racemic salts of methylethedrine,

where the molecule forms six "isostructural" groups, two of which were characterized by alternating motifs of H-bonding [106]. Analysis of co-crystals of meloxicam with carboxylic acids reveal the acids, which are able to break H-bonded meloxicam dimers, and, therefore, to compare the effect of crystal packing on dissolution behavior [107]. The comparison of crystal structures of hydrates of furosemide: Nicotinamide co-crystal suggests the mechanism of dehydration [108]. Galcera, et al. demonstrated by using this tool that the isostructurality in co-crystals of lamotrigin with flexible dicarboxilic acids appears at the presence of solvents able to mimic the difference in conformation and volume of co-formers [109]. The analysis of 42 tyrammonium salts demonstrated that isostructural cation packing can occur even with structurally different anions, with different hydration states and with different hydrogen bonding; realization of different packing was associated with various conformations of the ethylammonium group of the cation [110]. Martins, et al. demonstrated that similarity between supramolecular clusters occurs only for molecules able to exhibit similarity in molecular shape-size parameters (thus called isostructural molecules), contact area, and energy of intermolecular interactions [111]. Fenamate co-crystals with 4,4′-bipyridine keep the packing arrangement of the initial solid connected by the 4,4′-bipyridine [112]. The *Crystal Packing Similarity* tool was also used to investigate 16 trospium chloride containing structures. This molecule realizes similar conformation in the majority of solvates including a sesquihydrate, while its conformation in dihydrate significantly varies from that in other solvates. All solvates but water belong to the same group as two trospium chloride polymorphs [113]. Dehydration and desolvation of lenalidomide follow "isostructurality" in crystal packing: All solvates at heating convert to its' thermodynamically stable anhydrous form, whereas all hydrates upon dehydration convert to a metastable anhydrous polymorph able to transform upon further heating to the stable polymorph [114]. Analysis of H-bonding and crystal packing similarity for the crystal structures of vitamin D analogs showed that various conformations of its A-ring are predetermined by H-bonding of hydroxyl group both in crystals and in the binding pocket of the vitamin D receptor and that the exocyclic methylene group also influences H-bonding pattern in solids [66].

To sum up "isostructurality" found by means of the *CSD Crystal Packing Similarity* tool ignores the requirement for identical symmetry of compounds, and unit cell parameters. Instead, the families of structures with matching molecular clusters when superimposed can be found to reveal crystal packing relationships, motif stability, and hydrogen-bond competition for a variety of solid forms of a molecule (and its' homologues or structural analogs).

### *3.4. CSD-Crossminer*

The CSD-Crossminer is the novel software of the Cambridge Crystallographic Data Centre first appeared as part of the CSD-Enterprise in 2018. Its utility is based on ideas previously demonstrated on the example of carboxylate/tetrazolate [115], hydrate/peroxosovate [116], and maleate/saccharinate [82] behavior in solids and potential of 3D macrocyclic analogues of small-molecules to serve as drugs [117]. Particularly, molecules which form similar intermolecular interactions and have comparable size and shape tend to form similar supramolecular associates, and hence are able to form isotypical solvates, or bind with similar functional groups within a binding pocket of a macromolecule. A search defined within this software does not contain any chemical formulas or functional groups but uses such chemical feature as "H-bond donor", "H-bond acceptor", "hydrophobe", and others. Starting from a real molecule, mutual disposition of these chemical features can be defined, as well as the disposition of complementary functional features, which may come from other molecules, co-formers, solvates, or proteins and tolerance. The search is carried out within the CSD and the PDB databases and gives a number of hits potentially able to replace the reference molecule in solids or binding pockets. This software was developed as a pharmacophore query tool able to identify common protein binding sites in macromolecules, to determine structural motifs that are able to interact with similar binding sites, to estimate which ligand modifications are tolerated in a binding pocket, and others. More details about this tool are given in a white paper at *https://www.ccdc.cam.ac.uk/whitepapers/csd-crossminer-versatile-pharmacophore-query-tool-successful-modern-drug-discovery/*. However, the great potential of this tool

for material design should be mentioned. Using this tool, molecular templates for constructions of polynuclear complexes or porous compounds, like zeolites, can be found in the CSD (this means that these molecules not only possess a desired conformation, but also were once synthesized and isolated). As pores of metal–organic frameworks are somehow equivalent with the binding pockets, the potential of metal-organic frameworks in respect to catalysis, separation of complex mixtures, or host of guest molecules, can probably be evaluated using this software.

## 4. Solid Form Calculations

Calculations included within the CSD-Materials module of Mercury allows one to simulate crystal morphology using the BFDH (Bravais, Friedel, Donnay, and Harker) method, to perform semi-empirical MOPAC calculations and to evaluate force-field intermolecular energy calculations using the 'UNI' intermolecular potentials. The MOPAC software is a semi-empirical quantum chemistry program based on NDDO (neglect of diatomic differential overlap) approximation, which allows a user to perform some calculations (geometry optimization, bond order calculations, molecular electrostatic potential visualization) for isolated molecules. The 2007 or 2009 version can be obtained free for academic users at *http://openmopac.net/*. The application of intermolecular potentials for analysis of interactions between two molecules, of a molecular cluster, or of the total packing energy is beyond the scope of this review and will not be described here. See the description of the empirical "UNI" potentials and their possible applications with Refs. [118,119]. The BFDH morphology tool instead will be described in detail below.

### *4.1. BFDH Morphology Prediction*

Some of the macroscopic properties of solids depend on supramolecular architectures of symmetry elements formed by molecules and ions. Thus, if a supramolecular architecture is anisotropic, then, properties measured become anisotropic too; and their understanding and prediction require knowledge of disposition of functional groups, supramolecular synthons, or symmetry elements as compared with crystal faces. Having experimental data about Miller indices of crystal faces, one can examine corresponding planes using the free *Packing/Slicing tool* of Mercury. Particularly, indexing of the crystal phases becomes of practical interest for nonlinear optics [120], organic photonics [121], piezoelectrics [122–124], and organic electronics [125–128]. Knowledge of functional groups or supramolecular synthons forming crystal faces allowed in some cases to rationalize mechanical effects in dynamic crystals [129–132] such as self-healing, jumping, bending, twisting at heat, humidity, force or light, and to describe pressure-induced phase transitions (see Refs. [133–135] for analysis of such transitions in amino acids). Particle size and shape also affect material properties, such as tabletability [136], thus, their control is of special interest for the pharmaceutical industry.

Taking into account that the solvent can affect crystal morphology [137,138], it becomes of interest to rationalize solvent selection and to predict its' effect on crystal size and shape. Analysis of functional groups forming each surface gives a clue to solvent choice to prevent crystal growth in some directions, and vice versa, to rationalize the dissolution of a single crystal over various crystal faces [139]. For example, long-chain alkylboron capped tris-pyrazoloximates and clathrochelates readily form thin plate crystals with their main faces formed by hydrophobic alkyl groups (Figure 5) [140,141]. Their X-ray quality single crystals are obtained from polar solvents able to bind with small crystal faces formed by polar groups via hydrogen or halogen interactions, while crystallization from hydrocarbons typically results in twinned and turbostratic conglomerates of crystals. Similarly, ibuprofen [142] single crystals are faceted with (1 0 0), (0 0 2), and (0 1 1) faces, formed by hydrophobic, van der Waals and H-bonded interactions, respectively. As follows from the strength of intermolecular interactions in a crystal, and the strength of interactions between a solute and a solid [143], a polar protic solvent should bind to (0 0 2) faces to prevent the formation of needle morphology. This strategy based on the type of functional groups forming crystal faces was successfully used to optimize crystal morphology of lovastatin [144], 1-hydroxypyrene [145], isoniazid [146], tolbutamide [147] and N-benzyl-2-methyl-4-nitroaniline [148].

For phenacetin single crystals, the crash-cooling experiments resulted in the crystallization of needle-like crystals, while slow growth yielded similar single crystals with a hexagonal-like BFDH-predicted morphology affected by the solvent used [149]. Application of additive molecules able to bind with selected crystal faces also allows the of the controlling crystal morphology [150–153]. Yunqi Liu and coworkers suggested an interesting modification of such technique to affect the morphology and morphology-dependent breathing effect of metal–organic frameworks via the addition of a small amount of slightly modified ligands to the reaction mixture [154,155]. The hydrolysis of selected ligand decreased the growth of an anisotropic coordination polymer in some directions; the size of a crystal face containing pores was found to affect gas adsorption.

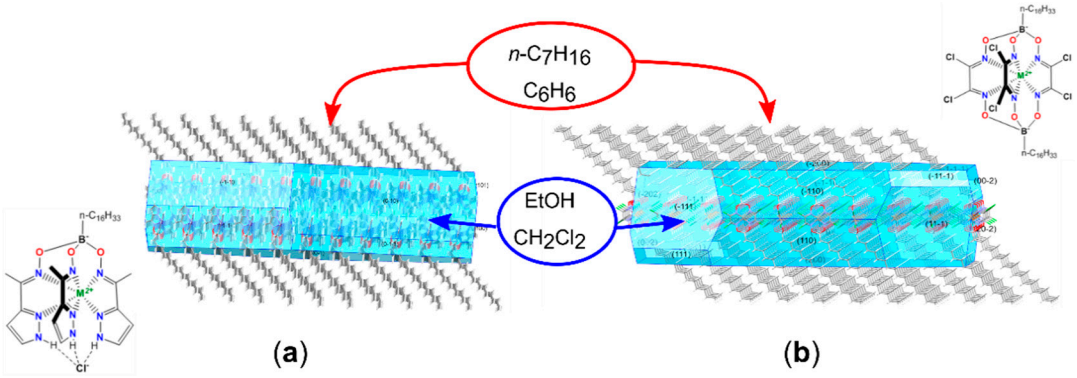


**Figure 5.** Bravais, Friedel, Donnay, and Harker **(**BFDH) predicted the morphology (blue) and hydrophobic groups forming the main crystal faces of a long-chain alkyl (**a**) tris-pyrazoloximate {1497845}, and (**b**) hexahalogenoclathrochelate {YUFYUV04}.

Having access to CSD-Materials, one can predict the morphology using the Bravais, Friedel, Donnay, and Harker (*BFDH*) crystal morphology tool (Figure 5). This method implies the idea that the crystals are preferable to grow along the direction with strong intermolecular interactions. Not only simulated but also experimental morphology can be depicted and analyzed to evaluate functional groups which form a crystal face and to estimate preferable interactions which occur between this face, a solvent, or an additive. Crystal morphology prediction can be used to estimate the direction of a preferred orientation for an experimental powder XRD patterns. Photomicrographs were taken during isothermal dehydration combined with calculated BFDH morphology to help distinguish concomitant polymorphs [156], to understand the faces, and directions of solvent loss [157], while atomic force microscopy supported with BFDH calculations was used to follow phase changes *in situ* [158]. Analysis of intermolecular interactions over molecular surfaces allows the rationalization of concomitant polymorphism of substances where single crystals of two crystal forms share faces of their crystals [159]. The case of intergrowth polymorphism [160,161] referred to the existence of two solid forms within one single crystal, which is a special case of such concomitant polymorphism. On the contrary, absence of similar surfaces on dominant phases of 1:1 and 3:2 co-crystals of *p*-toulenesulfonamide and triphenylphosphine oxide allowed Croker, et al. to conclude that solvent mediated phase transition in this system occurs through dissolving of one phase and re-crystallization of the other [162]. Analysis of polymorphs, solvates, and hydrates of trospium chloride containing structures demonstrated that these compounds can be divided into three main structural groups, and the predicted and experimental crystal morphology of various forms within one structural group was found to be very similar [113]. The BFDH morphology tool was applied to rationalize silicon oil induced spontaneous phase transition in ethynyl-substituted benzamides [163] and unusual mechanical response from a crystal undergoing topochemical dimerization [164].

More complex applications of BFDH morphology tool include synthesis of desired solid forms or prediction of desired properties for previously published compounds. It was shown that self-assembled monolayers of rigid biphenyl thiols [165–167] or silioxane-based monolayers [168,169] can be used as

templates to exclude concomitant polymorphysm (Figure 6a) or to obtain a metastable polymorph. First, analysis of crystal faces of the desired solid form was carried out to reveal functional groups on one of the main faces; then, the monolayer containing functional groups are able to form stable synthons with the above functional groups, which was used during crystallization (Figure 6b). Not only predesigned monolayers but also polymers [170,171] and additives (Figure 6c) [172,173] can be used as templates for crystallization. For example, β-1,4-saccharides act as templates to produce the metastable form III of paracetamol at crystallization from melt readily forming H-bonds with the (010) surface of form III [172], while the presence of sulfamides in solution promotes crystallization of γ-pyrazinamide from aqueous solutions [173]. Pyrazineamide usually nucleates from solutions in its' α form that contains molecular H-bonded dimers; amide of pyrazineamides probably forms heterodimers with sulfamide groups of templates on one of the crystal surfaces and then forms N-H...N connected chains with neighboring molecules. These chains are found only in γ-polymorph. Patel, Nguyen & Chadwick [171] not only used polymers to promote heterogeneous nucleation but also suggested to use *H-bonding propensities tool* to rank polymer surfaces towards heterogeneous nucleation of benzocaine and 1,1'-bi-2-naphthol.

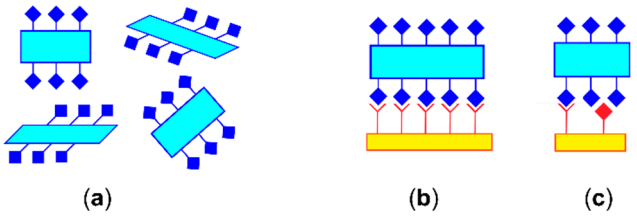


**Figure 6.** Schematic representation of (**a**) concomitant polymorphism, (**b**) crystallization on self-assembled monolayers, (**c**) crystallization on additives.

Applications of some anisotropic (needle, plate) crystals are related with anisotropy of chemical bonds within such solids. Anisotropic crystals with predominated faces formed by hydrophobic groups can be used as superhydrophobic porous materials [174]. Analysis of mechanical stimulus applied along three axes of unit cells to some layered energetic materials allows us to conclude that these explosives can convert kinetic energy into layer sliding to prevent the formation of hot spots [175]. This should also be the rationale for why high-performance insensitive energetic materials can be used as desensitizers versus mechanical stimuli. Vice versa, a corrugated molecular structure of celecoxib without any slip-planes and numerous weak interactions in orthogonal directions were suggested to be the reasons for exceptionally high elasticity of its needle singe crystals [176]. Flat naphthalene diimine derivatives were found to have comparable crystal packing governed by π...π stacking, similar crystal morphology, but exhibited various mechanical flexibility attributed to close packing or interlock of their terminal alkyl chains [177]. Investigation of sulfa drug crystals [178], co-crystals of vanillin isomers [179], and amino acids [180] demonstrated that H-bonded layered structures with orthogonal distribution of strong and weak interactions attain the feasibility of cleaving a crystal along a given crystallographic plane parallel with these robust synthons.Particularly, single crystals with molecular surfaces formed by hydrophobic interactions can be applied as clean surfaces for molecular beam epitaxy. The presence of slip planes is also thought to be associated with low elastic recovery upon compression, and greater plasticity [181,182]. Crystal morphology prediction was applied to discover new gelators by focusing on scaffolds with predicted high aspect ratio crystals [183].

Thus, analysis of crystal morphology and functional groups on main crystal faces cover many areas of crystal design and are important for many areas of industry. The tools implemented to the Mercury package can be helpful in these areas, but their application seems to be limited with anisotropic crystals or solids faceted with different functional groups. In other cases, this approach can be improved by DFT calculations of the interaction effect between the growing faces and the solvent molecules, or molecular electrostatic potential on crystal faces.

## 5. Knowlede-Based Prediction of Supramolecular Associates and Solid Forms

### *5.1. Polymorph Assessment*

Understanding and prediction of polymorphism—the ability of a solid material to exist in multiple crystal forms known as polymorphs—is vital for the industry as polymorphs of drugs, explosives, and pigments exhibit different properties [55]. It can be associated with various molecular conformations of flexible molecules, competing intermolecular interactions of polytopic molecules, various packing of molecules or supramolecular synthons, et cetera. While some paths to control polymorphism are described in Section 4.1, here, the approach to estimate the likelihoods of H-bonded polymorphism is described. It is of special interest for the analysis of compounds containing few donors (D) and acceptors (A) of H-bonding, since competition of donors or acceptors to take part in a hydrogen bond, and restrictions to form all highly likely bonds simultaneously may cause the appearance of polymorphs [184]. Taking into account that various polymorphs exhibit different properties including solubility, bioavailiability, tabletability, et cetera, the pharmaceutical industry has prompted the development of computational tools that are able to predict the likelihoods of H-bonded polymorphs. Thus, a methodology has been developed [185] to estimate the likelihood of H-bond formation for each pair of donors and acceptors in a molecule taking the environment of the D and A groups into account.

The *H-bond propensities tool* uses only a 2D molecular formula (Figure 7) and involves four stages: Data sampling, model fitting, model validation, and target assessment. For each functional group, it is either automatically assigned from the 2D formula, taken from the functional group library, or sketched manually by using a fitting data set, which is generated by loading in an existing set of structural data, or from the CSD. The H-bonds within the fitting data set are identified to collate statistics and descriptors of H-bonding formation. The logistic analysis is performed to generate a statistical model to determine the likelihood of H-bond formation; the model should be analyzed to include for the final model only significant variables and be good enough to proceed (area under ROC curve (receiver operating curve) above 0.8 indicates good discrimination). The results are ranked by propensity to allow inspection of the most and the least likely D-A pairs. Based on this knowledge-based approach, a structure that adopts the highest propensity H-bonds displays a low likelihood of appearance of a more stable polymorph, while for solid forms with lower propensities of H-bonds, a high risk of polymorphism caused by H-bonding is expected. For example, the most likely interaction for a "molecule" depicted in Figure 7 includes a donor atom of Group 3 and an acceptor atom of Group 1. However, in solid {Refcode} the second likely hydrogen bond between groups 1 and 2 is observed, thus, indicating possibility of appearance of another polymorph with the most likely hydrogen bond.

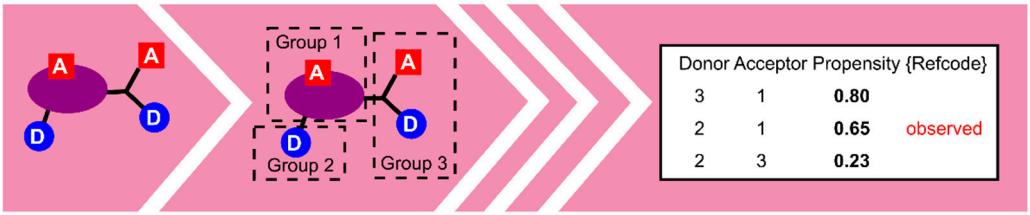


**Figure 7.** Flowchart for the methodology to predict the likelihood of hydrogen bond formation.

The tool has proved to be highly valuable in estimating the relative stability of known crystal forms [186]. Particularly, the kinetically more favored **Form I** of ritonavir displays statistically unlikely hydroxy-thiazoyl and ureido-ureido interactions but exhibits more favorable conformation of the carbamate moiety, while **Form II** realizes stronger hydrogen bonds as estimated in Ref. [186]. Two X-rayed polymorphs of 4-aminobenzoic acid realize different H-bonding, and the more stable form realizes more likely sets of H-bonding [187]. The approach was also successfully used to rationalize polymorphism for N2-(indol-3-acetyl)-L-aspargin [186], lamotrigine [188], and crizotinib [189,190] (see Figure 8 for chemical formulas of these compounds). Not only strong donors and acceptors of

H-bonding can be used for analysis; a competition of hydroxide O-H and ethynyl C−C≡C−H groups to form hydrogen bonds [191] and the role of $CHCl_3$ and $CH_2Cl_2$ molecules in crystal packing [192] were demonstrated using this tool.

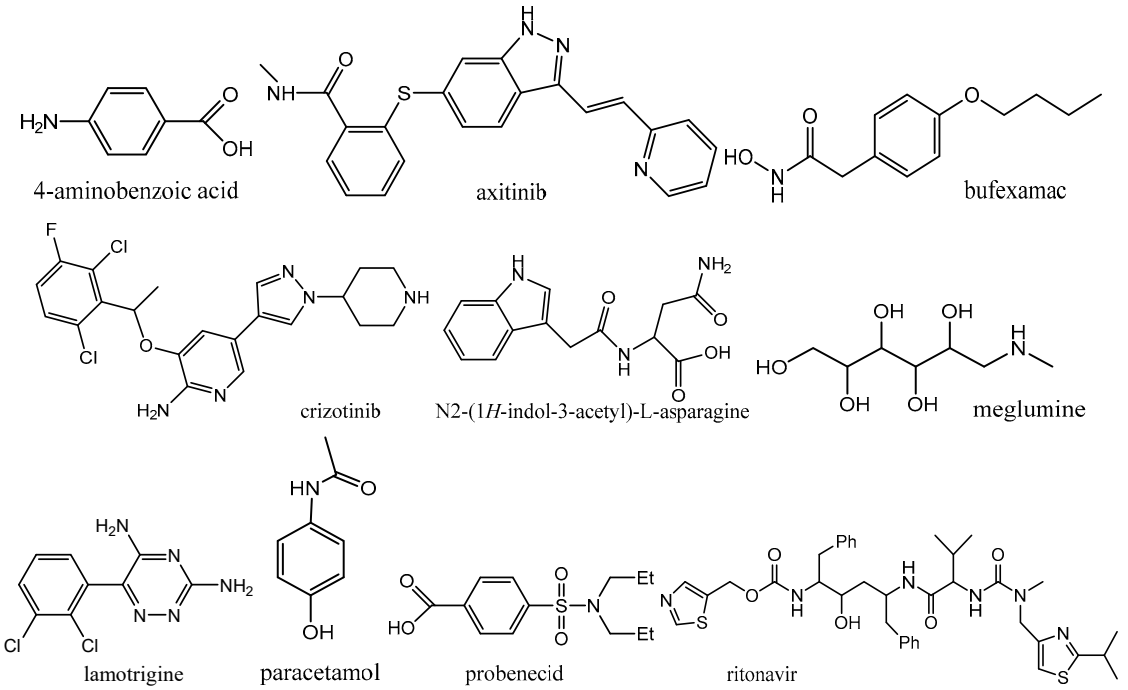


**Figure 8.** Schematic representation of compounds analyzed using H-bonding propensities tool.

Known forms of paracetamol both exhibit H-bonding between OH groups, that is a less likely donor to form a bond than an amide fragment. It was assumed that there was a conflict between a good donor group to form a bond disfavoring a poor acceptor to form bonding, which could be overcome by co-crystal formation with molecules containing the same D and A groups [187]. Indeed, co-crystals of paracetamol with diamino- or bis(4-pyridyl)-containing co-formers contain molecules of paracetamol connected by more likely amide/hydroxo or amide/amide pairs of interactions [193]. A good correlation between H-bonding charge analysis and H-bond propensities was also demonstrated for crizotinib [189], and heterocycle-1-carbohydrazoneamides [194].

Note, that the high probability for exhibiting polymorphism does not necessarily allow one to obtain novel polymorphs and that different polymorphs can realize the same H-bonds [195]. For example, probenecid was predicted to realize various H-bonded polymorphs, and differential scanning calorimetry indeed revealed three polymorphs, but XRD experiments showed that all of them realized the same hydrogen bonding [196]. For bufexamac, the propensity tool suggests the possible existence of three crystal forms, while Nauha and Bernstein found two polymorphs with similar H-bonds [197]. Two experimentally observed forms of meglumine realize slightly different H-bonding, which, however, are absent on putative structure landscape as these contain highly unlikely bifurcate acceptor OH groups [197]. For axitinib [189], five anhydrous polymorphs realize the most likely H-bonding, thus, the approach can not distinguish the most stable among them.

To sum up, the propensity tool neither predicts polymorphism, nor guarantees that all sets of theoretically possible H-bonding combinations can be obtained or guidelines can be given on how to obtain any of these polymorphs. It does not describe inclinations of a molecule to form concomitant polymorphs, conformational polymorphs, or packing polymorphs, or solid forms with Z' >1. Instead, it indicates the possibility of solid forms to organize various H-bonded architectures and provides some guidelines on the amount of affords that one can spend in the experimental search for various crystal forms. Abramov also notes such a limitation of the approach as incapability to distinguish more stable

polymorph among crystal forms with similar H-bonded networks, which however can be overcome with additional charge-density analysis of known polymorphs [189]. At the same time, its application is not limited by monomolecular systems. Note, that any desired functional groups, additional co-formers, and solvent molecules can be included in the statistical model. Thus, although this method is not able to predict the ratio of components in a co-crystal, it can be applied for co-crystal design.

### *5.2. Co-Crystals Design*

Co-crystals are solids that consist of two and more components (co-formers) that form a unique crystalline structure having unique properties. Thus, co-crystallization is an approach to optimize the physical properties of solid materials. For example, pharmaceutical co-crystals can be obtained to modulate dissolution rate and physical stability of drugs [198,199]. Schultheiss and Neuman reported [200] the effect of coformers on melting points, stability towards humidity, solubility, bioavailiability, and some other properties of pharmaceutical co-crystals. Karki, et al. [201] demonstrated that the tabletability of pharmaceuticals can be tuned up on the example of paracetamol co-crystals with various co-formers. The dependence of mechanical properties of acid...amid based co-crystals was studied by Saha and Desiraju [202]. The potential of co-crystallization for tuning the properties of the energetic materials [175,203,204], optical materials [205,206], and for the food industry [207] have also been demonstrated in recent papers. In contrast with synthetic routes focused on the synthesis of covalent derivatives containing functional groups that affect the desired property, co-crystallization became of interest as a 'greener' process, frequently free of toxic ingredients and by-products. Pharmaceutical compounds in this context become of particular interest as these molecules contain functional groups that can be involved in molecular recognition of biomolecules [208]. The main task of crystal chemistry in this field is to estimate which co-formers, if any, will form a co-crystal with a given molecule prior to screening and investigation of properties of the solid obtained.

One group of methods available are quantum chemical calculations from simple energy minimization to full structure prediction [209]. Another group of methods is based on data knowledge about the likely homo and heterosynthons. Since the works of Etter [210], it is known that (i) all good donors and acceptors tend to take part in hydrogen bonding, (ii) the strongest donors tend to interact with the strongest acceptors. In this context, it becomes essential for a researcher to estimate which donors and acceptors are "good" and "the strongest". The *H-bonding propensities* tool allows ranking of various donors and acceptors without any quantum-chemical calculations (Figure 9).

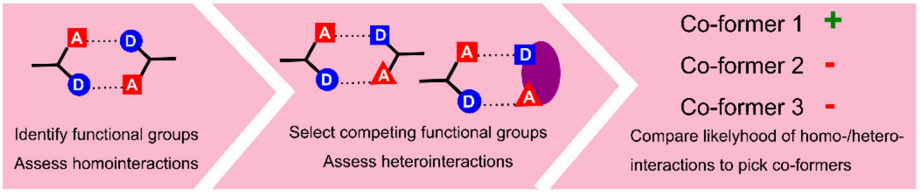


**Figure 9.** Flowchart for co-crystal design strategies based on synthon competition.

*H-bonding propensities* tool for uncharged and charged molecules of pyrimethamine and dicarboxylic acids, as well as halogenated aromatic compounds (Figure 10a), was successful in predicting formation and non-formation of adducts [211]. A similar approach was later applied to pyrimethamine with some other drug molecules also taking solvent molecules into account [212]. Note, that proton transfer accompanied with transformation of a co-crystal to a salt was rationalized in terms of their $\Delta pK_a$ values [213,214], where $\Delta pK_a = pK_a$[protonated base] − $pK_a$[acid] >2 or 3 was found for salts, negative $\Delta pK_a$ was characteristic of co-crystals, while an intermediate situation may result in both depending on stable supramolecular synthons [215]. Hydrogen-bond propensities gave similar trends as calculated bond energies for possible synthons in thiazole amides (Figure 10b), and co-crystallization of six thiazole amides with 20 different carboxylic acids demonstrated effectiveness of complimentary energy-based and data–knowledge predictions for the prediction of likely synthons [216].

The knowledge-based approach to co-crystal design was successfully applied to select pyrazinoids and pyridinoids as prospective co-formers for a diuretic drug hydrochlorothiazide [217] to tune its solubility. The amide-pseudoamide synthon was shown to be more stable than the formation of two dimers of the theophylline molecule, that allowed to explain the formation of theophylline: Amide co-crystals [218]. At the same time, theophylline co-crystals with fluorobenzoic acids demonstrate that it is still difficult to predict co-crystallization of small rigid molecules using this method [219]. Similarly, preferable co-crystallization of only one of three tautomers of 2-amino-6-methyl-1,4-dihydropyrimidin-4-one with carboxylic acids was explained using this approach [220]. Potential of co-crystal design for molecules with limited H-bonding functionalities was demonstrated on the example of propyphenazone [221]: $NH_2$, OH, and $CO_2H$ functionalities were found to be the most likely groups to interact with O=C group, and eight novel co-crystals were obtained using co-formers containing OH or/and $CO_2H$ groups. Dicarboxylic acids [222] or anions [223,224] can be applied to co-crystallize two molecules, which do not form co-crystals.

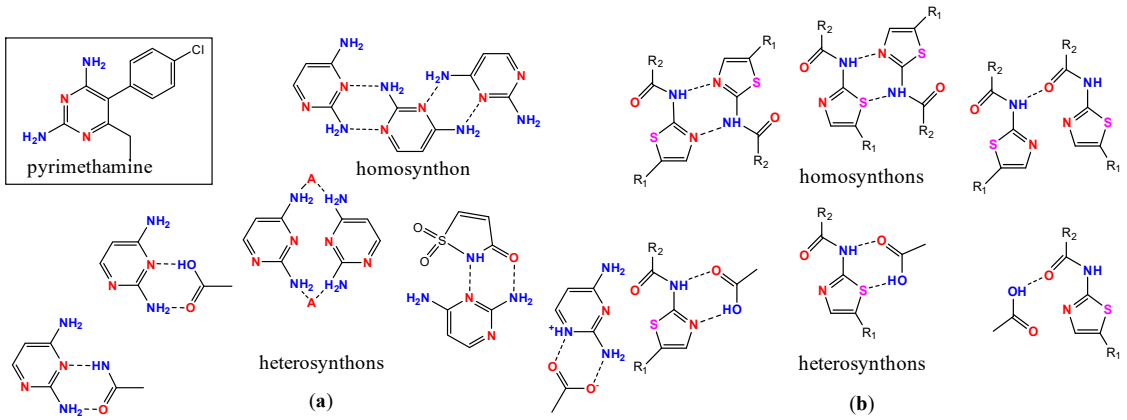


**Figure 10.** Examples of homo/heterosynthons analyzed for (**a**) pyrimethamine [211,212], and (**b**) thiazole-amides [216].

Note, that the analysis of possible heterosynthons is not limited to co-crystals. It can be utilized to investigate inclusion compounds [225] and mixtures of polymers and solutes [171]. Besides, the ranking of heterosynthons on their relative strength can not only help in estimating the most likely binary co-crystals. This method has great potential in the synthesis of multicomponent co-crystals based on polytopic co-formers. Thus, H-bonded heterosynthons are able to interact with the third co-former through halogen bonds [226–228]. π-Stacking in conjunction with hydrogen bonding was used for synthesis of ternary co-crystals [229,230]. Combination of H-bonded synthons and stacking interactions between donor and acceptor planar molecules allowed Desiraju and co-workers to synthesize quaternary and even quintinary co-crystals [231,232]. Partial substitution of some co-formers in quaternary systems with their shape-size analogs even allowed for obtaining six component solids [233].

Although some examples of co-crystals design based on H-bonding propensities tool are given above, successful prediction of inclination of some molecules to form co-crystals obviously needs analysis of some other molecular descriptors. First, the possibility of a solvent to take part in H-bonding should be taken into account [211,212,234]. A systematic study of co-crystallization of paracetamol with H-bond acceptors [235] and donors [236] demonstrated that paracetamol molecules in these crystals are linked via either OH···O=C or NH···O=C interactions, depending on the presence or absence of substituent groups on the molecule of the second co-crystal former. A machine learning algorithm trained out on a set of paracetamol co-crystal experiments using more than 190 molecular descriptors for each co-former allowed to predict 9 of the 13 experimentally obtained co-crystals within the top 11 suggestions [237]. Unfortunately, this method requires a large amount of experimental work to train the model, and the model obtained should be applied only to molecules with similar molecular

descriptors as those for an attested molecule. Fabian has proposed a methodology that involves using size and shape complementarity as the primary driver for co-crystal formation [238]. Analysis of 131 molecular descriptors for 710 co-crystal partners suggested that co-crystals were more likely to form between molecules of a similar size and shape and with a similar polarity of co-crystal formers, thus both these descriptors were recently included to the *Co-Crystal Design tool*.

Effectiveness of such modification can be demonstrated on the example of 1,2,4-thiadiazole derivative co-crystallization with gallic and vanillic acids [239]. While *H-bonding propensities tool* gives almost equal probability of occurrence of homo- and heterosynthons, molecular complementarity tool indicates that co-crystals in these systems should form; and these co-crystals were experimentally obtained. Karki, et al. [240] demonstrated that synthon analysis combined with Fabian's methodology was effective in prediction of possible co-formers for artemisinin. A series of co-crystals of sulfamethoxazole [241] and leflunomide [242] were synthesized using this approach. Prediction of possible H-bonded motifs between tyraminium cations and violurate anions also successfully predicted many of the bimolecular synthons experimentally observed in tyraminium violurate polymorphs and hydrates, but also demonstrated that none of the trimolecular synthons were predicted [243]. Note, that tri- and tetra-molecular synthons are not something unusual in co-crystals (see, for example, tetramolecular associates found in thiazole-amides, Figure 10), thus any predictions should also include such polymolecular associates into account.

To sum up, *H-bonding Propensities* and *Co-Crystal Design* tools allow one to simplify co-crystal screening. CSD analysis helps to select complementary functional groups to form heterosynthons more likely to form than homosynthons. Presence of false positives in experimental screening then may be accounted for other factors. For example, although hydrogen bonds are thought to be stronger than halogen bonding, one can undergo a competitive co-crystallization between H-bonded and halogen bonded synthons based on the polarity of a solvent used [244]. It was shown that in polar solvents 1,2-bis(pyrid-4-yl)ethane forms co-crystals via halogen bonds, and in nonpolar - via H-bonds. Of more concern with regards to co-former screening is the possibility of false negatives. If the results of this type of analysis are used to narrow down the number of screening experiments performed, any possible co-crystals that are incorrectly marked as unlikely to form would be missed. Besides quantum calculations of molecular dimers or logistic models trained on large datasets of co-crystals, development of shape-size molecular complementarity tools for the prediction of possible co-formers seem to be very promising. Note, that the CSD-Crossminer package developed for sophisticated search of analogues of drugs is now available (Section 3.4). It utilizes the idea that molecules with similar disposition of functional groups and hydrophobic fragments may act similarly with proteins and replace each other. The idea of substitution of one of the co-crystal formers with its size-shape analog can be realized using this program.

### *5.3. Full Interaction Maps*

The *Full Interaction Maps* (FIM) tool [245] implemented within the Mercury package visualizes the likelihood of a synthon appearance and corresponding geometry variation between functional groups of a molecule under consideration, and a probe functional group. For each functional group of a molecule, 3D scatterplots of CSD contact searches with a chosen probe, and the functional groups are generated and converted into scaled density maps. These density maps are then combined for the whole molecule, taking the environmental effects of combinative factors and steric exclusion to account. The 2019 version of the CSD-Enterprise contains (i) $RNH_3$, uncharged and charged NH nitrogen atoms as probe functional groups of donors of hydrogen bonds, (ii) various oxygen atoms (of a carbonyl and alcohol group or a water molecules) as a probe of hydrogen bond acceptors, (iii) methyl and aromatic carbon atoms as a probe of stacking interactions. The CSD-Enterprise version of 2018 allowed the use of C-I and C-Br interactions as a probe of (iv) halogen interactions; and the next year these interactions were extended with C-F and C-Cl probes, to evaluate differences between various halogen atoms. For each functional group, the FIM distribution is similar with *IsoStar* scatterplots of corresponding

functional groups, but the FIM for a whole molecule reflects the fact that some of functional groups are better donors and acceptors of, for example, H-bonding, than the others. On these maps, this difference is expressed in the color (and the coordinates of the most likely positions of the donor and acceptor sites can be additionally calculated and depicted), while corresponding quantitative values can be estimated using the *H-bonding Propensities* tool (Section 5.1). Besides, these maps are very sensitive to the steric exclusion from other molecular species and would differ for a molecule in optimized and experimental geometries, and those obtained with CSD-Conformer Generator.

The FIMs probed with H-bond donors (blue) and acceptors (red) and supramolecular synthons of the *Pbcn* polymorph of chalcone {BZYACO01}and 5-(4-bromophenyl)-1-phenylpent-2-en-4-yn-1-one {YILNAK} are depicted in Figure 11. For both molecules' blue regions near the ketone oxygen atom reflect its inclination to form bifurcate bonding due to the presence of two lone pairs on the oxygen atoms. The most expected positions of acceptors of hydrogen bonding for the chalcone are situated on the opposite sites of the molecule, and correlate well with observed supramolecular synthons in its polymorphs—a dimer depicted in Figure 11, a {BZYACO01}and a head-to-tail chain {BZYACO04} similar with that of 5-(4-bromophenyl)-1-phenylpent-2-en-4-yn-1-one. Elongation of the π-conjugated chain with a triple bond makes the appearance of such chains more abundant than dimer occurrence (Figure 11b), that was experimentally confirmed for a series of 1,5-diarylpent-2-en-4-yn-1-ones [246,247].

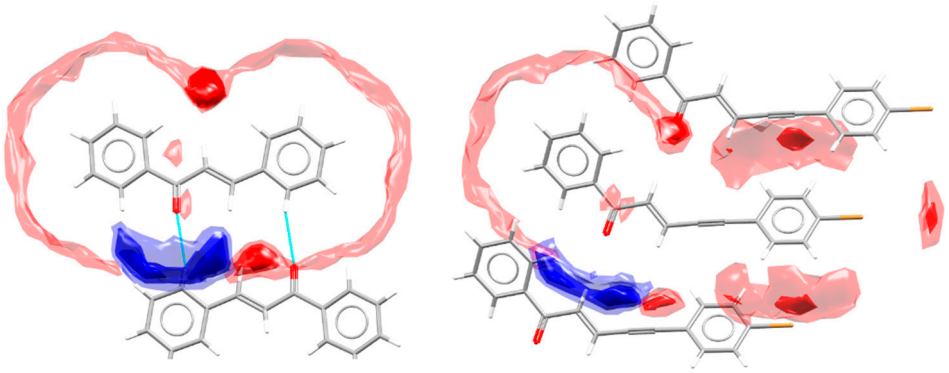

(**a**) (**b**)

**Figure 11.** Interaction maps and supramolecular synthons in the crystal structures of (**a**) chalcone {BZYACO01}, (**b**) (E)- 5-(4-bromophenyl)-1-phenylpent-2-en-4-yn-1-one {YILNAK}.

This tool has been applied mainly for the analysis of strong hydrogen bonds [54,170,190,194,248–251] in accord with the first test functional groups suggested within this tool, and the first paper published to describe it. Mutual disposition of hot spots can be used to find functional groups of the same molecule [245], co-formers [243,249,250], active sites in a binding pocket of a macromolecule [252], or surface inhibitors [170], which match a given pattern of interaction preferences. Analysis of polymorphs of some drugs demonstrated that disposition of H-bond donors and acceptors close to the hotspots are indicative for the more stable polymorph even if a molecule realizes less likely conformation [190]. However, in the case of polymorphism induced by weak intermolecular interaction reorganization [253] or high-pressure [254], it has lower predictive ability. This can easily be understood if we keep in mind that data for the FIMs are plotted based on structural information derived at atmospheric pressure.

At the same time, the test carbonyl oxygen and uncharged NH groups can be successfully applied to reveal positions of acceptors and donor of C-H...O [170,255–257] and C-H...N [258] bonding. It was demonstrated in Refs. [255,257] that the FIMs can be applied to estimate likely C-H...O bonded motifs for chalcones, polyenones, pentenynones and cyclic ketones with vinylacetylene fragments. At the same time, it was demonstrated that C=O and C-Br groups compete with each other for the most acidic hydrogen atoms, thus that FIM predictions of synthons based on C-H...Br bonding became less reliable at the presence of C-H...O=C bonding [257]. At the absence of carbonyl groups the FIMs

for the N-salicilidenanylines probed with C-I and C-F groups successfully predict all of the C-I...N and many of the C-F...H-C interactions in co-crystals of N-salicilidenanylines with perhalogenated co-formers [259]. Mugheirbi and Tajber analyzed the FIM hotspots around the itraconazole molecule to understand the molecular environment in the mesophase [260]. The itraconazole lacks any donors of strong H-donors but has a number of competing acceptors of H-bonding; thus, analysis of the FIMs and FTIR spectra allowed them to reveal the most ordered of mesophases, and to propose that the greatest mobility of this molecule is associated with movement of the triazoline ring. Analysis of FIMs in two polymorphs of the dinuclear Co(II)-Shiff base complex revealed the most acidic H(C) atoms (similar in both polymorphs), which take part either in C-H...O bonding in the triclinic polymorph, or in the C-H...π bonding in the monoclinic polymorph, or even to not take part in any prominent intermolecular bonding [256].

Note, that unsatisfied strong acceptors observed in a crystal structure solved from powder XRD data may be indicative of missed water/solvent [261,262]. In this case coordinates of the most expected position of a water molecule can be used in the refinement. Worth noting, that *IsoStar* and FIMs deal only with intermolecular interactions but a similar idea could be used for investigation of metal-ligand bonding in polytopic ligands. This could be helpful for understanding the factors that govern linkage isomerism, and to estimate the most likely coordination mode of the most widespread ligands.

### *5.4. CSD-Conformer Generator*

Representation of a molecule in the three-dimensional space finds numerous applications in structure solution from powder diffraction data in real space, crystal structure prediction including the formation of co-crystals, protein–ligand docking, and others. Thus, the *CSD-Conformer Generator* tool included in the CSD-Enterprise as an approach to a fast generation of plausible molecular conformations by using geometric distributions derived from the CSD. First, for the input 3D molecular model with all hydrogen atoms present, all bond lengths and angles are minimized based on corresponding average values. Then, the molecule is partitioned into rotamers, and rotamer libraries and ring template libraries are used to generate a conformer tree with unforbidden and preferred rotatable bond geometries and ring geometries. A final set of conformers is clustered according to conformer similarity. Each conformer is locally optimized in torsion space. It was demonstrated that this tool reproduced well conformations of a number of molecules observed in the CSD and the Protein Data Bank [263,264]. Some discrepancies between the predicted and experimental geometries occurred for the ligand: Macromolecule complexes in unusual conformational space, rare rotamer examples, uncertain bond types, and some other cases, nevertheless, theoretical configuration space represents well experimental data [265,266] or configurations obtained by the Molecular Operating Environment's Low Mode Molecular Dynamics module [267]. It was demonstrated that the CSD-Conformer Generator combined with ab initio [268] or DFTB3-D3 [269] calculations can be used for crystal structure prediction of some flexible pharmaceuticals. Such combination reproduced well the molecular geometry and crystal parameters, although did not provide sufficiently accurate energy ranking.

## 6. Hydrate/Solvate Analyser

As it was described above, a solvent can affect crystal morphology and sometimes determines the polymorph, but it also can be built into the crystal structure to form a hydrate or solvate. Since water is nature's solvent, non-toxic and widespread, the scientific community is interested in understanding water assembles in liquids and solids. In particular, medium-sized and large water clusters are important for biology, since they act as surrounding and solvating solutes for biologically active molecules, fill discrete voids and channels in molecular and supramolecular assemblies including their reactive sites and interpenetrate into the interfacial region of hydrophobic surfaces [270–273]. Besides, water associates are involved in dynamic processes such as proton transport, material or molecular folding, de/resolvation, and others [274,275], and even affect mechanical properties of single crystals [276]. The behavior of liquid and solid water including ice, clathrates, and ice-like systems are

determined by the disorder of the hydrogen atoms, and the binding energy of different configurations as well as some other properties can also differ [277–279]. At last, but not least different solvents may stabilize different forms of a molecule (the neutral or zwitterionic forms) [280,281]. In other words, both (i) connectivity of a solvent molecule in a crystal, inclination to form a given associate, and (ii) dimensionality and unit cell volume that goes to solvents are of interest for biology, crystallography, and material chemistry. All corresponding algorithms are realized within the *Hydrate* and *Solvate Analyser* tools of the CSD-Material module. The *Hydrate Analyser* provides information about the water H-bond geometry and motifs (one of any of 10 most common motifs described by Ref. [282]) detected, information on the volume occupied with water molecules, and display the water space and water interaction maps. The *Solvate Analyser* provides similar information about simple and mixed solvates, co-formers and ions.

### *6.1. Analysis of the Local Connectivity of a Solvent*

Analysis of solvate connectivity and the most abundant motifs (if any) formed by solvent molecules is similar to that described above for the investigation of other synthons and supramolecular associates. The practical meaning of results obtained for material chemistry, biochemistry, and the pharmaceutical industry are based on the fact that similar hydrate architectures were found in crystals of both inorganic, organic, coordination, and even macromolecular compounds [40,41]. H-bonding between a complex and an outer sphere solvent can lead to additional quenching in luminescent materials that are unfavorable for the task-specific design of optical materials [283,284]. Comparison of clathrate, turbolato-clathrate, and non-clathrate hydrates revealed that water associates in the latter can be regarded as fragments of clathrate hydrates [285]. Analysis of hydrate architectures in crystal structures of known kosmotropic and chaotropic agents revealed that the kosmotropes tend to take part in H-bonding with hydrates, while chaotropes in crystals tend to from clathrate hydrate-like structures [286]. Kosmotropic agents are those able, by the ordering of the water structure in solution, to enhance intermolecular interactions within protein molecules, thus preventing denaturation, while chaotropes act oppositely. Hence, the property of a molecule to crystallize with water giving full enclathration was directly associated with the ability to act as chaotrope.

Most frequently water serves as a donor of two hydrogen bonds and an acceptor of one hydrogen bond, although three other motifs are also relatively common (Figure 12a [282,287,288]). The dual nature of this molecule in respect to H-bonding allowed proposing imbalance in the number of donor and acceptor groups of a polytopic molecule to be the reason for form hydrate appearance [289]. Although, it is in accordance with Etter's rule, which states that "all good proton donors and acceptors are used in hydrogen bonding" [210], Infantes, Fábián, and Motherwelldemonstrated that the imbalance of donor and acceptor groups, in fact, does not affect inclination of a molecule to form hydrates [288]. Instead, it more readily interacts with unsatisfied acceptors of H-bonding, especially $R_2PO_2^-$, $Cl^-$, $C\text{-}NH_3^+$ groups, acts as a bridge between unsatisfied donors and acceptors, and occupies the free volume, especially for chiral molecules [290]. The strong imbalance between the number of donors and acceptor groups between tetrasulfonate-functionalized rigid anions and planar polyamino-containing cations indeed afforded their crystallization as hydrates, where water molecules act both as bridges between cations and anions, and clusters incorporated within cavities and channels of H-bonded networks [251]. Nevertheless, typically it is still hardly possible to predict if a compound will form a hydrate or not. Zaworotko and coworkers revealed that not only molecules with unsatisfied donors but also acceptors of H-bonding also readily form hydrates, but the reason of CSD statistics, in this case, might underestimate inclination of a molecule to form a hydrate, probably, because the most effective pathways to hydrate formation were slurrying in water and exposure to humidity [291]. The role of MeOH [292], DMSO [293,294], and $CHCl_3$ and $CH_2Cl_2$[192] solvates in crystals was also investigated.

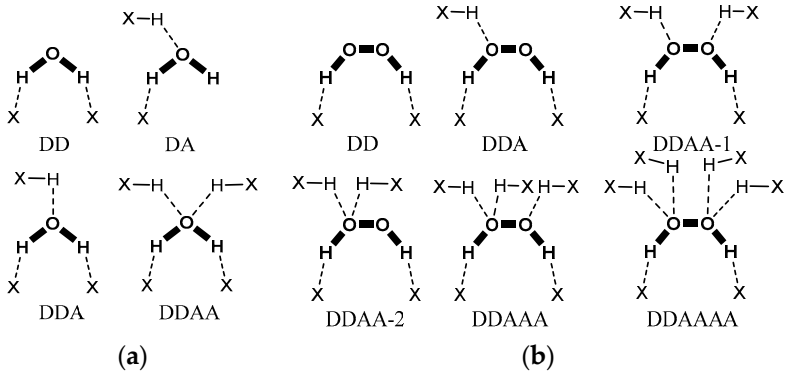


**Figure 12.** H-bonding patterns in (**a**) organic hydrates [288] and (**b**) organic peroxosolvates [116] (X denotes any donor or acceptor atom).

Comparison of motifs formed by water molecules in organic hydrates and by $H_2O_2$ in organic peroxosolvates gave a clue to the understanding of their isomorphysm [116,295]. It was found that $H_2O_2$ always forms two H-bonds as a proton donor, and up to four bonds as an acceptor of H-bonding (Figure 12b). Thus, only three of the peroxosolvate H-bonding patterns are similar to those observed in crystals of hydrates. As isomorphous substitution may occur only in crystals with similar H-bonding motifs, peroxosolvates with DD, DDA, and DDAA motifs connectivity require high $H_2O_2$ concentrations for synthesis, are sensitive to humidity, and as a result are of limited practical meaning. Instead, peroxosolvates involved in at least five hydrogen bonds and strong H-bonding with acceptors are not inclined to take part in isomorphous substitution with hydrates.

Not only water connectivity, but also the main motifs formed by water molecules, or supramolecular architectures including water molecules as well as suggested nomenclature were described [67]. Combined together, these data have practical meaning for prediction of coordinates of missing water molecules for solving and refinement of crystal structures from powder X-Ray diffraction data [261], as well as for molecular docking with GOLD (Genetic Optimization for Ligand Docking), part of the CSD-Discovery module.

### *6.2. Analysis of Solvent Associates*

Thus, besides analysis and classification of H-bonded motifs, visualization of associates, and calculation of the unit cell volume occupied with water/solvent molecules (both coordinated and not) is available via *Hydrate/Solvate Analyser* tool. On Figure 13, a DMSO and water space in the structure of bosutinib DMSO solvate trihydrate {ABECES} are shown in red and blue, respectively. It is clearly seen that both solvents form isolated clusters, while in the structure of tetrabutylammonium fluoride clathrate hydrate {CIPRAV} H-bonded water molecules form a 3D architecture with tetrabutylammomium cations situated in pores of this framework (Figure 13b). Visualization is similar to void analysis, but there is no need to remove any molecules to carry out calculations. Moreover, the *Solvate analyser* tool can be used to identify not only solvents, but also co-formers and ions, disordered fragments, or even hydrophobic/hydrophilic fragmentset cetera, as well as to visualize their packing and check H-bonding involving the identified components.

Analysis of the voids within previously published copper-containing coordination polymers allowed Inokuma et al. to find a crystalline sponge with desired pore size and affinity to guest molecules and demonstrated that a huge number of previously published coordination polymers can be used to capture guest molecules [296]. Anisotropic motifs formed by solvent molecules affect mechanical properties of compounds, and dehydration mechanism. For example, presence of infinite H-bonded water chains is typically associated with the reversible dehydration process and similarity between crystal structures of the hydrated and anhydrous forms of a solid, like caffeine [297], carbamazepin [104], aspartame [298], and Shiff-base Ni(II) complex [299]. Such channels can be not only dehydrated but also substituted with other solvents [300,301]. The solid dehydration with

prominent atomic movement traced with single-crystal or powder X-Ray diffraction can shed light on a more complex mechanism of water loss [302–306]. Various mobility of the water clusters incorporated within the pores and H-bonding waters that structure these pores was demonstrated in Refs. [251,307]. Liu et al. demonstrated that anhydrous uric acid and its' dihydrate exhibited various mechanical properties of their single crystals despite the similarity of layered motifs formed by the acid [276]. 2D water associates situated between acid layers perpendicular with single crystal main faces break at indentation with dehydration at crystal surface and make this solid softer than the anhydrous form.

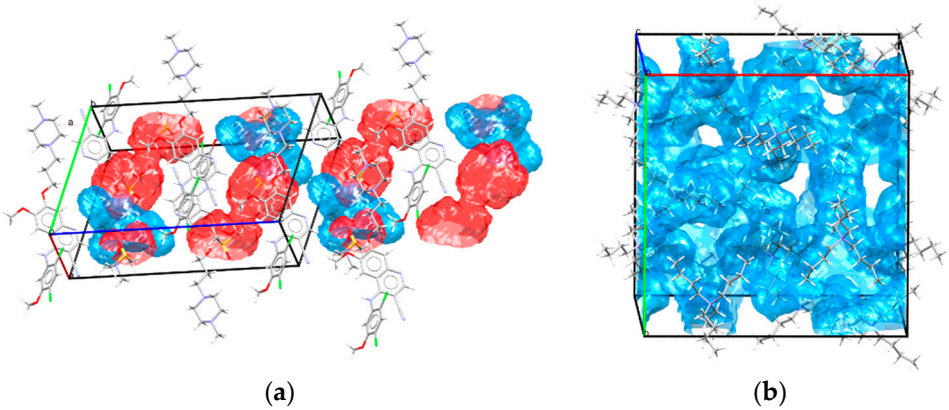

(**a**) (**b**)

**Figure 13.** The structure of (**a**) bosutinib dimethyl sulfoxide (DMSO) solvate trihydrate {ABECES} and (**b**) tetrabutylammonium fluoride clathrate hydrate {CIPRAV} with solvate analyser display of DMSO space shown in red and water space in light blue.

## 7. Additional Software Compatible with the CSD-Materials Analysis of Structure–Property Networks

### *7.1. CSD Python API*

The *CSD Python API* is now part of the CSD-Enterprise automatically installed as part of the CSD installation. This allows one to run supplied or user-written Python scripts for the loaded structure or a set of structures. CCDC Python-Built-In scripts include at the moment:

- Analysis (generation of conformers and calculation of their RMSD (*conformes_similarity.py*) or of all torsion angles (*generate_conformers.py*) for the loaded structure).
- External *(load_in_conquest.py*– loading the current structure into the ConQuest sketch window).
- Reports (generating a report in *.html format containing crystallographic details, molecular geometry, and intermolecular hydrogen and halogen bonding (*crystal_structure_report.py*), or molecular geometry, including Mogul geometry analysis (*molecular_geometry_report.py*), or crystal packing descriptors (*quick_packing_check.py*), or basic chemical, crystallographic and publication information about the loaded structure (*structure-simple_report.py*)).
- Searches within the CSD for entries relevant to the specified chemical name or synonym (*chemical_name_search.py*) or having similar molecular geometry (*molecular_similarity_search.py*).
- One can additionally download from the CSD-Python API Forum [308] the following scripts:
- To generate molecular formula and weight (*welcome-and-weight.py*), Crystal14 input files (*crystal_inputs.py*) or Packing Similarity dendrogram (*Packing_Similarity_Dendrogram.py*);
- To send a Mol2 or CIF files to an external application (*send_mol2_to_notepad+.py*);
- To generate diagrams for all molecules in a structure file (*diagram_to_file.py*);
- To find covalently bonded clusters within a structure (*dimensionality.py*);
- To perform void calculation in a crystal (*void_calc.py*);
- To merge GOLD docking results (*gold_merge.py*);
- To filter molecular conformers with unusual torsion angles (*conformer_filter_density.py*);

- To extract from the CSD unique rings of a specified size (*ring_type_count.py*);
- To compare protein bound ligand with CSD-Generated conformers (*find_binding_conformation.py*).

Some other examples of Python scripts applied for investigation of crystal structures include removing solvent molecules from a MOF subset extracted from the CSD to perform analysis of geometry and properties of nondisordered porous compounds [309]; authors realized the possibility to remove by request both uncoordinated and coordinated solvent molecules from coordination polymers. Dolinar et al. wrote a Python script to perform the CSD search of chiral monomolecular compounds [310]. Bryant, Maloney, and Sykes investigated a number of polymorphs and co-crystals with previously reported tabletabilities to analyze how different factors govern tabletability of organic crystals, and to suggest a programmatic method to calculate corresponding crystal descriptors [311]. Their investigation of the most likely slip planes, their interpenetration on connection by weaker interactions, presence of other slip planes, and automatic assessment of H-bond dimensionalities revealed that the degree of separation, followed by the presence of H-bonds between the layers, and finally d-spacing between potential slip planesare the most important descriptors affecting the tabletability. The corresponding CSD Python API protocol that can be applied for the prediction of mechanical properties of organic crystals was also published [311]. Miklitz and Jelfs reported a Python script for structural analysis of porous materials (organic and coordination cages) that estimates the cavity diameter, number of windows, and their diameter [312]. It uses Cartesian coordinates and atom types for input, thus, can be in principle applied also to selected fragments of framework materials. Besides codes to extract and analyze data stored within the CSD, for text mining of selected properties within a large set of papers was also published [313]. The algorithm uses manuscript html files as input for extraction of surface areas and pore volumes of metal–organic frameworks with at least 73% accuracy and can be used for investigation of structure–property networks.

Thus, the Python API gives a convenient path to combine and modify the CSD requests with CSD-Materials, CSD-Discovery tools or external software for ones' purposes. The next Section gives some examples of the combination of the CSD-Materials tools with external crystallographic software.

### *7.2. Combination of Various Tools and Algorythms*

Some combinations of the CSD-Materials tools with external software were mentioned in previous Sections, for example, the combination of the *CSD Conformer Generator* with periodic calculations to predict crystal structures, or that of the *CSD Co-Crystal Former* and the *H-bond propensities* with DFT calculations to better understand competing for intermolecular interactions. Let us mention also some other examples, where the *CSD-Materials* tools were used in unusual way or as the tool to solve only part of a scientific problem.

Crystal packing of organic single-component compounds with Z′ = 1 were compared to evaluate the effect of chemical transformation on crystal packing and isostructurality using a combination of the CSD Python API scripts, external software, and the *CSD Crystal Packing Similarity* tool [85]. For this purpose, 15,5543 organic compounds were extracted from the CSD based on their composition and data quality. Then, a freely available algorythm published in 2010 [314] was used to cleave up to three acyclic single bonds between functional groups as demonstrated in Figure 14. Comparison of the *Crystal Packing Similarity* between molecular clusters formed by the "Value" molecular parts, allows us to reveal the most frequent terminal transformations of the "Key" groups and to evaluate their effect of the packing and isostructurality. For example, substitution of the methyl group to the chloro-, azide- or iodo- groups gives isostructural pairs in nearly 30% of cases.

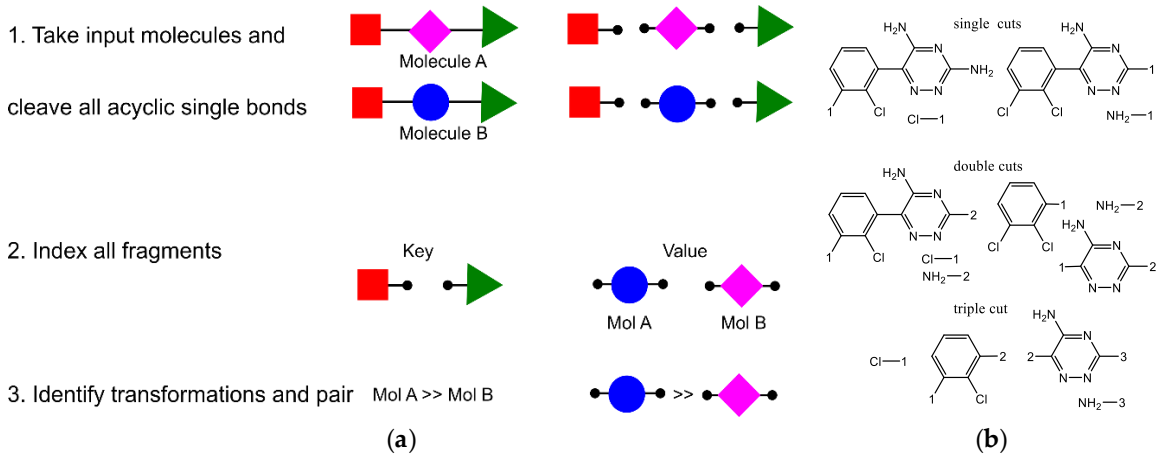


**Figure 14.** (**a**) Flowchart of the algorythm of bond cleavage reported at Refs. [85,314] and (**b**) some fragments formed from single, double, and triple cuts of lamotrigine.

Recently possibility of prediction of H-bonded motifs using a topological approach was demonstrated for some families of organic molecules with a large number of X-rayed representatives [315,316]. This method schematically represented in Figure 15 utilizes the idea that (i) only a limited number of architectures can be formed from a particular building block with a given connectivity, (ii) overall topology of a network depends on connectivity of building blocks, and (iii) propensities of various networks appearance are not equal. While relations between connectivity of an organic molecule and resulting network and corresponding propensities of their appearance have already been published [315,317], this approach does not allow evaluating the most abundant molecular connectivity of insufficiently studied families of organic compounds. Recently, maps of electrostatic potential, the *Full Interaction Maps*, and the *H-bonding Propensities* were compared as the tools to overcome this problem for heterocycle-1-carbohydrazoneamides [194]. Knowledge-based approaches demonstrated competition between various nitrogen atoms to act as acceptors of H-bonding with the donor -$NH_2$ group and allowed evaluating local molecular connectivity. Experimental crystal structures realize one of highly abundant theoretically predicted topologies of an H-bonded network.

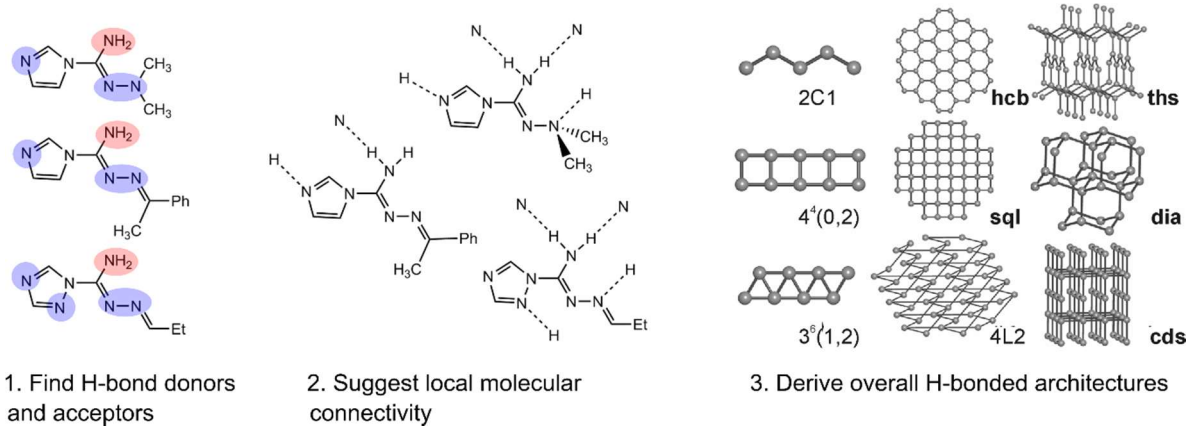


**Figure 15.** Flowchart of the algorithm to estimate H-bonding architectures of organic molecules.

Tilbury, et al. suggested to combine the *H-bond propensity* based prediction with COSMO-RS theory [318,319] to predict drug substance hydrate formation [320]. Hydrate formation probability is estimated based on propensities calculated for each donor/acceptor groups in drug...drug or drug...water pairs. The most favorable hydrate formation has the maximal difference between these values. Although within this model relative strength of different functional groups to interact

with water is displayed, this model does not take steric effects and intramolecular interactions into account. Additional quantum mechanics approach to eliminate donor and acceptor groups that are unable to form intermolecular interactions and to calculate the most favorable molecular and hydrate conformations allowed to improve predictive fidelity of calculations.

Chandra, et al. [225] applied CSD to enhance the solubility of telmisartan (TEL), a low soluble antihypertensive drug. First, the possibility of TEL to form likely intermolecular interactions with sulfobutylether beta-cyclodextrin was confirmed using H-bonding propensities tool. Then, the best docking pose of an inclusion complex of TEL in cyclodextrine was found with GOLD. The predicted binding mode was in line with the experimental spectra for the inclusion complex, which demonstrated enhanced solubility and dissolution rate of TEL.

Correlation between solubility and various parameters describing dimethyl sulfoxide (DMSO) role in crystals structures was carried out by Spitery, et al. [294]. They analyzed various parameters of hydrogen bonding of DMSO molecules as obtained from crystal structures reported in the CSD with solubility estimated using Chem3D [321], and found a negative correlation between the number of interactions the solvent is involved in and solubility of a solid.

## 8. Conclusions

The Cambridge Crystallographic Data Center holds a unique position of a curator of the Cambridge Crystallographic Database that now contains more than 10,000,00 crystal structures and a software developer for the analysis of collected data. This software allows the visualization of complex statistical data in a click-of-a-button manner (*Full Interaction Maps, Conformer Generator, Mogul analysis, Solvate Analyzer, BFDH predictions*), and investigation of local connectivity of functional groups and small molecules (*H-Bond Propensities, Co-Crystal Former, Motif Search*) that became possible due to the network between chemical diagrams and automatically calculating interatomic and intermolecular distances. Despite the complexity of the utilized algorithms, big data analysis, and their sophisticated processing, the software remains visible, user-friendly, and available for each CSD user. Thus, its' visibility and flexibility combined with exhaustive free documentation (see user guides, how-to-video, tutorials, and other materials at [322]) provide the basis for successful application in crystal engineering, material chemistry, and chemoinformatics.The diversity of CSD-supported studies described in this review indicate the great potential of the knowledge-based software for future development in these and associated fields, thus, the development of links with other molecular and crystallographic databases and repositories of properties would be advantageous.

The combination of the CSD tools with external software similarly with UNI and MOPAC calculations incorporated within the CSD-Enterprise seems to be very prospective for future development. DFT calculations, especially periodic ones, could provide further insight into the field of coordination polymers with numerous applications in gas storage and separation, catalysis, and spintronics. Implementation of graph theory to polytopic molecules and ligands could expand data about the local (molecular) connectivity to knowledge about possible and most abundant coordination and H-bonded architectures. The future of this field still possesses many challenges, but there is no denying that the value of the Cambridge Structural Database and associated software for the knowledge-based analysis in the filed of composition–structure–properties studies can not be overestimated.

**Funding:** This work was supported by the Ministry of Science and Higher Education of the Russian Federation.

**Acknowledgments:** The author is grateful to A. A. Korlyukov for fruitful discussion of the text.

**Conflicts of Interest:** The author declares no conflict of interest.

## References


1. Allen, F.; Kennard, O.; Watson, D.; Brammer, L.; Orpen, A.; Taylor, R. Tables of Bond Lengths Determined by X-Ray and Neutron-Diffraction .1. Bond Lengths in Organic-Compounds. *J. Chem. Soc.-Perkin Trans. 2* **1987**, S1–S19. [CrossRef]
2. Orpen, A.; Brammer, L.; Allen, F.; Kennard, O.; Watson, D.; Taylor, R. Tables of Bond Lengths\Determined by X-Ray and Neutron-Diffraction .2. Organometallic Compounds and Co-Ordination Complexes of the D-Block and F-Block Metals. *J. Chem. Soc.-Dalton Trans.* **1989**, S1–S83. [CrossRef]
3. Allen, F.H.; Kennard, O.; Taylor, R. Systematic analysis of structural data as a research technique in organic chemistry. *Acc. Chem. Res.* **1983**, *16*, 146–153. [CrossRef]
4. Allen, F.H.; Kirby, A.J. Bond length and reactivity. Variable length of the carbon-oxygen single bond. *J. Am. Chem. Soc.* **1984**, *106*, 6197–6200. [CrossRef]
5. Kitaigorodskii, A.I. *Molecular Crystals and Molecules*; Academic Press: New York, NY, USA, 1973.
6. Desiraju, G.R.; Parshall, G.W. *Crystal Engineering: The Design of Organic Solids*; Elsevier: Amsterdam, The Netherlands, 1989.
7. Lehn, J.-M. *Supramolecular Chemistry: Concepts and Perspectives*; Wiley-VCH: Weinheim, Germany, 1995.
8. Nangia, A.K.; Desiraju, G.R. Crystal Engineering: An Outlook for the Future. *Angew. Chem. Int. Ed.* **2019**, *58*, 4100–4107. [CrossRef]
9. Corpinot, M.K.; Bučar, D.-K. A Practical Guide to the Design of Molecular Crystals. *Cryst. Growth Des.* **2019**, *19*, 1426–1453. [CrossRef]
10. Duggirala, N.K.; Perry, M.L.; Almarsson, Ö.; Zaworotko, M.J. Pharmaceutical cocrystals: Along the path to improved medicines. *Chem. Commun.* **2015**, *52*, 640–655. [CrossRef]
11. Zhang, J.; Xu, W.; Sheng, P.; Zhao, G.; Zhu, D. Organic Donor–Acceptor Complexes as Novel Organic Semiconductors. *Acc. Chem. Res.* **2017**, *50*, 1654–1662. [CrossRef]
12. Shi, P.-P.; Tang, Y.-Y.; Li, P.-F.; Liao, W.-Q.; Wang, Z.-X.; Ye, Q.; Xiong, R.-G. Symmetry breaking in molecular ferroelectrics. *Chem. Soc. Rev.* **2016**, *45*, 3811–3827. [CrossRef]
13. Turkoglu, G.; Cinar, M.E.; Ozturk, T. Triarylborane-Based Materials for OLED Applications. *Molecules* **2017**, *22*, 1522. [CrossRef]
14. Kidyarov, B.I. Comparative Interrelationship of the Structural, Nonlinear-Optical and Other Acentric Properties for Oxide, Borate and Carbonate Crystals. *Crystals* **2017**, *7*, 109. [CrossRef]
15. Quan, L.N.; Rand, B.P.; Friend, R.H.; Mhaisalkar, S.G.; Lee, T.-W.; Sargent, E.H. Perovskites for Next-Generation Optical Sources. *Chem. Rev.* **2019**, *119*, 7444–7477. [CrossRef] [PubMed]
16. Mackenzie, C.F.; Spackman, P.R.; Jayatilaka, D.; Spackman, M.A. CrystalExplorer model energies and energy frameworks: Extension to metal coordination compounds, organic salts, solvates and open-shell systems. *IUCrJ* **2017**, *4*, 575–587. [CrossRef] [PubMed]
17. Carugo, O.; Blatova, O.A.; Medrish, E.O.; Blatov, V.A.; Proserpio, D.M. Packing topology in crystals of proteins and small molecules: A comparison. *Sci. Rep.* **2017**, *7*, 13209. [CrossRef]
18. Taylor, R.; Wood, P.A. A Million Crystal Structures: The Whole Is Greater than the Sum of Its Parts. *Chem. Rev.* **2019**, *119*, 9247–9477. [CrossRef] [PubMed]
19. Groom, C.R.; Allen, F.H. The Cambridge Structural Database in Retrospect and Prospect. *Angew. Chem. Int. Ed.* **2014**, *53*, 662–671. [CrossRef]
20. Groom, C.R.; Bruno, I.J.; Lightfoot, M.P.; Ward, S.C. The Cambridge Structural Database. *Acta Cryst. Sect. B* **2016**, *72*, 171–179. [CrossRef] [PubMed]
21. Belsky, A.; Hellenbrandt, M.; Karen, V.L.; Luksch, P. New developments in the Inorganic Crystal Structure Database (ICSD): Accessibility in support of materials research and design. *Acta Cryst. Sect. B* **2002**, *58*, 364–369. [CrossRef] [PubMed]
22. Berman, H.M.; Westbrook, J.; Feng, Z.; Gilliland, G.; Bhat, T.N.; Weissig, H.; Shindyalov, I.N.; Bourne, P.E. The Protein Data Bank. *Nucleic Acids Res.* **2000**, *28*, 235–242. [CrossRef]
23. Peresypkina, E.V.; Blatov, V.A. Topology of molecular packings in organic crystals. *Acta Cryst. Sect. B* **2000**, *56*, 1035–1045. [CrossRef]
24. Peresypkina, E.V.; Blatov, V.A. Molecular coordination numbers in crystal structures of organic compounds. *Acta Cryst. Sect. B* **2000**, *56*, 501–511. [CrossRef] [PubMed]

25. Pathaneni, S.S.; Desiraju, G.R. Database analysis of Au···Au interactions. *J. Chem. Soc. Dalton Trans.* **1993**, 319–322. [CrossRef]
26. Terrasson, V.; Planas, J.G.; Prim, D.; Teixidor, F.; Viñas, C.; Light, M.E.; Hursthouse, M.B. General Access to Aminobenzyl-o-carboranes as a New Class of Carborane Derivatives: Entry to Enantiopure Carborane–Amine Combinations. *Chem.—A Eur. J.* **2009**, *15*, 12030–12042. [CrossRef] [PubMed]
27. Thomas, S.P.; Pavan, M.S.; Row, T.N.G. Experimental evidence for 'carbon bonding' in the solid state from charge density analysis. *Chem. Commun.* **2013**, *50*, 49–51. [CrossRef] [PubMed]
28. Alkorta, I.; Del Bene, J.E.; Elguero, J. $H_2XP{:}OH_2$ Complexes: Hydrogen vs. Pnicogen Bonds. *Crystals* **2016**, *6*, 19. [CrossRef]
29. Lodochnikova, O.A.; Latypova, L.Z.; Madzhidov, T.I.; Chmutova, G.A.; Voronina, J.K.; Gubaidullin, A.T.; Kurbangalieva, A.R. "Lp···synthon" interaction as a reason for the strong amplification of synthon-forming hydrogen bonds. *CrystEngComm* **2019**, *21*, 1499–1511. [CrossRef]
30. Taylor, R. Which intermolecular interactions have a significant influence on crystal packing? *CrystEngComm* **2014**, *16*, 6852–6865. [CrossRef]
31. Taylor, R. It Isn't, It Is: The C–H···X (X = O, N, F, Cl) Interaction Really Is Significant in Crystal Packing. *Cryst. Growth Des.* **2016**, *16*, 4165–4168. [CrossRef]
32. Jelsch, C.; Ejsmont, K.; Huder, L. The enrichment ratio of atomic contacts in crystals, an indicator derived from the Hirshfeld surface analysis. *IUCrJ* **2014**, *1*, 119–128. [CrossRef]
33. Jelsch, C.; Bibila Mayaya Bisseyou, Y. Atom interaction propensities of oxygenated chemical functions in crystal packings. *IUCrJ* **2017**, *4*, 158–174. [CrossRef]
34. Buergi, H.B.; Dunitz, J.D. From crystal statics to chemical dynamics. *Acc. Chem. Res.* **1983**, *16*, 153–161. [CrossRef]
35. Bürgi, H.-B.; Dunitz, J.D. *Structure Correlation*; Wiley-VCH: Weinheim, Germany, 1994.
36. Vologzhanina, A.V.; Korlyukov, A.A.; Antipin, M.Y. Special features of intermolecular bonding A···D (A = Si, Ge and D = nucleophile) in crystal structures. *Acta Cryst. Sect. B* **2008**, *64*, 448–455. [CrossRef] [PubMed]
37. Bruno, I.J.; Cole, J.C.; Kessler, M.; Luo, J.; Motherwell, W.D.S.; Purkis, L.H.; Smith, B.R.; Taylor, R.; Cooper, R.I.; Harris, S.E.; et al. Retrieval of Crystallographically-Derived Molecular Geometry Information. *J. Chem. Inf. Comput. Sci.* **2004**, *44*, 2133–2144. [CrossRef] [PubMed]
38. Bruno, I.J.; Cole, J.C.; Lommerse, J.P.M.; Rowland, R.S.; Taylor, R.; Verdonk, M.L. IsoStar: A library of information about nonbonded interactions. *J. Comput. Aided Mol. Des.* **1997**, *11*, 525–537. [CrossRef] [PubMed]
39. McKenzie, J.; Feeder, N.; Hunter, C.A. H-bond competition experiments in solution and the solid state. *CrystEngComm* **2016**, *18*, 394–397. [CrossRef]
40. Mascal, M.; Infantes, L.; Chisholm, J. Water Oligomers in Crystal Hydrates—What's News and What Isn't? *Angew. Chem. Int. Ed.* **2006**, *45*, 32–36. [CrossRef] [PubMed]
41. Manna, U.; Halder, S.; Das, G. Ice-like Cyclic Water Hexamer Trapped within a Halide Encapsulated Hexameric Neutral Receptor Core: First Crystallographic Evidence of a Water Cluster Confined within a Receptor-Anion Capsular Assembly. *Cryst. Growth Des.* **2018**, *18*, 1818–1825. [CrossRef]
42. Desiraju, G.R. Supramolecular Synthons in Crystal Engineering—A New Organic Synthesis. *Angew. Chem. Int. Ed.* **1995**, *34*, 2311–2327. [CrossRef]
43. Aakeröy, C.B. Crystal Engineering: Strategies and Architectures. *Acta Cryst. Sect. B* **1997**, *53*, 569–586. [CrossRef]
44. Hollingsworth, M.D. Crystal Engineering: From Structure to Function. *Science* **2002**, *295*, 2410–2413.
45. Nagarathinam, M.; Peedikakkal, A.M.P.; Vittal, J.J. Stacking of double bonds for photochemical [2+2] cycloaddition reactions in the solid state. *Chem. Commun.* **2008**, 5277–5288. [CrossRef] [PubMed]
46. Ramamurthy, V.; Sivaguru, J. Supramolecular Photochemistry as a Potential Synthetic Tool: Photocycloaddition. *Chem. Rev.* **2016**, *116*, 9914–9993. [CrossRef] [PubMed]
47. Kreuer, K.-D. Proton Conductivity: Materials and Applications. *Chem. Mater.* **1996**, *8*, 610–641. [CrossRef]
48. Horiuchi, S.; Kumai, R.; Tokura, Y. Hydrogen-Bonding Molecular Chains for High-Temperature Ferroelectricity. *Adv. Mater.* **2011**, *23*, 2098–2103. [CrossRef] [PubMed]
49. Horiuchi, S.; Noda, Y.; Hasegawa, T.; Kagawa, F.; Ishibashi, S. Correlated Proton Transfer and Ferroelectricity along Alternating Zwitterionic and Nonzwitterionic Anthranilic Acid Molecules. *Chem. Mater.* **2015**, *27*, 6193–6197. [CrossRef]

50. Horiuchi, S.; Kagawa, F.; Hatahara, K.; Kobayashi, K.; Kumai, R.; Murakami, Y.; Tokura, Y. Above-room-temperature ferroelectricity and antiferroelectricity in benzimidazoles. *Nat. Commun.* **2012**, *3*, 1308. [CrossRef] [PubMed]
51. Owczarek, M.; Hujsak, K.A.; Ferris, D.P.; Prokofjevs, A.; Majerz, I.; Szklarz, P.; Zhang, H.; Sarjeant, A.A.; Stern, C.L.; Jakubas, R.; et al. Flexible ferroelectric organic crystals. *Nat. Commun.* **2016**, *7*, 13108. [CrossRef] [PubMed]
52. Borel, C.; Larsson, K.; Håkansson, M.; Olsson, B.E.; Bond, A.D.; Öhrström, L. Oxalate- and Squarate-Biimidazole Supramolecular Synthons: Hydrogen-Bonded Networks Based on $[Co(H_2biimidazole)_3]^{3+}$. *Cryst. Growth Des.* **2009**, *9*, 2821–2827. [CrossRef]
53. Pallipurath, A.R.; Civati, F.; Eziashi, M.; Omar, E.; McArdle, P.; Erxleben, A. Tailoring Cocrystal and Salt Formation and Controlling the Crystal Habit of Diflunisal. *Cryst. Growth Des.* **2016**, *16*, 6468–6478. [CrossRef]
54. George, F.; Norberg, B.; Wouters, J.; Leyssens, T. Structural Investigation of Substituent Effect on Hydrogen Bonding in (S)-Phenylglycine Amide Benzaldimines. *Cryst. Growth Des.* **2015**, *15*, 4005–4019. [CrossRef]
55. Bernstein, J. *Polymorphism in Molecular Crystals*; Oxford University Press: Oxford, UK, 2007.
56. Bauer, J.; Spanton, S.; Henry, R.; Quick, J.; Dziki, W.; Porter, W.; Morris, J. Ritonavir: An Extraordinary Example of Conformational Polymorphism. *Pharm. Res.* **2001**, *18*, 859–866. [CrossRef] [PubMed]
57. Dalinger, I.L.; Vatsadze, I.A.; Shkineva, T.K.; Kormanov, A.V.; Struchkova, M.I.; Suponitsky, K.Yu.; Bragin, A.A.; Monogarov, K.A.; Sinditskii, V.P.; Sheremetev, A.B. Novel Highly Energetic Pyrazoles: N-Trinitromethyl-Substituted Nitropyrazoles. *Chem.—Asian J.* **2015**, *10*, 1987–1996. [CrossRef] [PubMed]
58. Dalinger, I.L.; Kormanov, A.V.; Suponitsky, K.Y.; Muravyev, N.V.; Sheremetev, A.B. Pyrazole-Tetrazole Hybrid with Trinitromethyl, Fluorodinitromethyl, or (Difluoroamino)dinitromethyl Groups: High-Performance Energetic Materials. *Chem.—Asian J.* **2018**, *13*, 1165–1172. [CrossRef] [PubMed]
59. Dalinger, I.L.; Serushkina, O.V.; Muravyev, N.V.; Meerov, D.B.; Miroshnichenko, E.A.; Kon'kova, T.S.; Suponitsky, K.Y.; Vener, M.V.; Sheremetev, A.B. Azasydnone—Novel "green" building block for designing high energetic compounds. *J. Mater. Chem. A* **2018**, *6*, 18669–18676. [CrossRef]
60. Bredikhin, A.A.; Bredikhina, Z.A.; Zakharychev, D.V. Crystallization of chiral compounds: Thermodynamical, structural and practical aspects. *Mendeleev Commun.* **2012**, *22*, 171–180. [CrossRef]
61. Bredikhin, A.A.; Zakharychev, D.V.; Bredikhina, Z.A.; Kurenkov, A.V.; Krivolapov, D.B.; Gubaidullin, A.T. Spontaneous Resolution of Chiral 3-(2,3-Dimethylphenoxy)propane-1,2-diol under the Circumstances of an Unusual Diversity of Racemic Crystalline Modifications. *Cryst. Growth Des.* **2017**, *17*, 4196–4206. [CrossRef]
62. Kinbara, K.; Hashimoto, Y.; Sukegawa, M.; Nohira, H.; Saigo, K. Crystal Structures of the Salts of Chiral Primary Amines with Achiral Carboxylic Acids: Recognition of the Commonly-Occurring Supramolecular Assemblies of Hydrogen-Bond Networks and Their Role in the Formation of Conglomerates. *J. Am. Chem. Soc.* **1996**, *118*, 3441–3449. [CrossRef]
63. Haynes, D.A.; Chisholm, J.A.; Jones, W.; Motherwell, W.D.S. Supramolecular synthon competition in organic sulfonates: A CSD survey. *CrystEngComm* **2004**, *6*, 584–588. [CrossRef]
64. da Silva, C.C.P.; de Oliveira, R.; Tenorio, J.C.; Honorato, S.B.; Ayala, A.P.; Ellena, J. The Continuum in 5-Fluorocytosine. Toward Salt Formation. *Cryst. Growth Des.* **2013**, *13*, 4315–4322. [CrossRef]
65. Chisholm, J.A.; Motherwell, S. COMPACK: A program for identifying crystal structure similarity using distances. *J. Appl. Cryst.* **2005**, *38*, 228–231. [CrossRef]
66. Wanat, M.; Malinska, M.; Kutner, A.; Wozniak, K. Effect of Vitamin D Conformation on Interactions and Packing in the Crystal Lattice. *Cryst. Growth Des.* **2018**, *18*, 3385–3396. [CrossRef]
67. Infantes, L.; Motherwell, S. Water clusters in organic molecular crystals. *CrystEngComm* **2002**, *4*, 454–461. [CrossRef]
68. Blatov, V.A.; O'Keeffe, M.; Proserpio, D.M. Vertex-, face-, point-, Schläfli-, and Delaney-symbols in nets, polyhedra and tilings: Recommended terminology. *CrystEngComm* **2009**, *12*, 44–48. [CrossRef]
69. Batten, S.R.; Champness, N.R.; Chen, X.-M.; Garcia-Martinez, J.; Kitagawa, S.; Ohrstrom, L.; O'Keeffe, M.; Suh, M.P.; Reedijk, J. Terminology of metal–organic frameworks and coordination polymers (IUPAC Recommendations 2013). *Pure Appl. Chem.* **2013**, *85*, 1715–1724. [CrossRef]
70. Ohrstrom, L. Designing, Describing and Disseminating New Materials by using the Network Topology Approach. *Chem.—Eur. J.* **2016**, *22*, 13758–13763. [CrossRef] [PubMed]

71. Bonneau, C.; O'Keeffe, M.; Proserpio, D.M.; Blatov, V.A.; Batten, S.R.; Bourne, S.A.; Lah, M.S.; Eon, J.-G.; Hyde, S.T.; Wiggin, S.B.; et al. Deconstruction of Crystalline Networks into Underlying Nets: Relevance for Terminology Guidelines and Crystallographic Databases. *Cryst. Growth Des.* **2018**, *18*, 3411–3418. [CrossRef]
72. Haneline, M.R.; Tsunoda, M.; Gabbaï, F.P. π-Complexation of Biphenyl, Naphthalene, and Triphenylene to Trimeric Perfluoro-ortho-phenylene Mercury. Formation of Extended Binary Stacks with Unusual Luminescent Properties. *J. Am. Chem. Soc.* **2002**, *124*, 3737–3742. [CrossRef] [PubMed]
73. Burress, C.; Elbjeirami, O.; Omary, M.A.; Gabbaï, F.P. Five-Order-of-Magnitude Reduction of the Triplet Lifetimes of N-Heterocycles by Complexation to a Trinuclear Mercury Complex. *J. Am. Chem. Soc.* **2005**, *127*, 12166–12167. [CrossRef] [PubMed]
74. Taylor, T.J.; Burress, C.N.; Gabbaï, F.P. Lewis Acidic Behavior of Fluorinated Organomercurials. *Organometallics* **2007**, *26*, 5252–5263. [CrossRef]
75. Ferraris, J.; Cowan, D.O.; Walatka, V.; Perlstein, J.H. Electron transfer in a new highly conducting donor-acceptor complex. *J. Am. Chem. Soc.* **1973**, *95*, 948–949. [CrossRef]
76. Giri, G.; Verploegen, E.; Mannsfeld, S.C.B.; Atahan-Evrenk, S.; Kim, D.H.; Lee, S.Y.; Becerril, H.A.; Aspuru-Guzik, A.; Toney, M.F.; Bao, Z. Tuning charge transport in solution-sheared organic semiconductors using lattice strain. *Nature* **2011**, *480*, 504–508. [CrossRef] [PubMed]
77. Varghese, S.; Das, S. Role of Molecular Packing in Determining Solid-State Optical Properties of π-Conjugated Materials. *J. Phys. Chem. Lett.* **2011**, *2*, 863–873. [CrossRef] [PubMed]
78. Zou, T.; Wang, X.; Ju, H.; Zhao, L.; Guo, T.; Wu, W.; Wang, H. Controllable Molecular Packing Motif and Overlap Type in Organic Nanomaterials for Advanced Optical Properties. *Crystals* **2018**, *8*, 22. [CrossRef]
79. Larin, A.A.; Muravyev, N.V.; Pivkina, A.N.; Suponitsky, K.Y.; Ananyev, I.V.; Khakimov, D.V.; Fershtat, L.L.; Makhova, N.N. Assembly of Tetrazolylfuroxan Organic Salts: Multipurpose Green Energetic Materials with High Enthalpies of Formation and Excellent Detonation Performance. *Chem.—Eur. J.* **2019**, *25*, 4225–4233. [CrossRef] [PubMed]
80. Dolgushin, F.M.; Smol'yakov, A.F.; Suponitsky, K.Y.; Vologzhanina, A.V.; Fedyanin, I.V.; Shishkina, S.V. Intermolecular interactions in polymorphs of the cyclic trimeric perfluoro-ortho-phenylene mercury from geometric, energetic and AIM viewpoints: DFT study and Hirshfeld surface analysis. *Struct. Chem.* **2016**, *27*, 37–49. [CrossRef]
81. Torubaev, Y.V.; Rai, D.K.; Skabitsky, I.V.; Pakhira, S.; Dmitrienko, A. Energy framework approach to the supramolecular reactions: Interplay of the secondary bonding interaction in $Ph_2E_2$ (E = Se, Te)/p-I-$C_6F_4$-I co-crystals. *New J. Chem.* **2019**, *43*, 7941–7949. [CrossRef]
82. Martins, F.T.; Paparidis, N.; Doriguetto, A.C.; Ellena, J. Crystal Engineering of an Anti-HIV Drug Based on the Recognition of Assembling Molecular Frameworks. *Cryst. Growth Des.* **2009**, *9*, 5283–5292. [CrossRef]
83. Pogoda, D.; Janczak, J.; Videnova-Adrabinska, V. New polymorphs of an old drug: Conformational and synthon polymorphism of 5-nitrofurazone. *Acta Cryst. Sect. B* **2016**, *72*, 263–273. [CrossRef]
84. Reilly, A.M.; Cooper, R.I.; Adjiman, C.S.; Bhattacharya, S.; Boese, A.D.; Brandenburg, J.G.; Bygrave, P.J.; Bylsma, R.; Campbell, J.E.; Car, R.; et al. Report on the sixth blind test of organic crystal structure prediction methods. *Acta Cryst. Sect. B* **2016**, *72*, 439–459. [CrossRef]
85. Giangreco, I.; Cole, J.C.; Thomas, E. Mining the Cambridge Structural Database for Matched Molecular Crystal Structures: A Systematic Exploration of Isostructurality. *Cryst. Growth Des.* **2017**, *17*, 3192–3203. [CrossRef]
86. Carletta, A.; Colaço, M.; Mouchet, S.R.; Plas, A.; Tumanov, N.; Fusaro, L.; Champagne, B.; Lanners, S.; Wouters, J. Tetraphenylborate Anion Induces Photochromism in N-Salicylideneamino-1-alkylpyridinium Derivatives Through Formation of Tetra-Aryl Boxes. *J. Phys. Chem. C* **2018**, *122*, 10999–11007. [CrossRef]
87. Nath, N.K.; Saha, B.K.; Nangia, A. Isostructural polymorphs of triiodophloroglucinol and triiodoresorcinol. *New J. Chem.* **2008**, *32*, 1693–1701. [CrossRef]
88. Moorthy, J.N.; Mandal, S.; Venugopalan, P. Hydrogen-Bonded Helical Self-Assembly of Sterically-Hindered Benzyl Alcohols: Rare Isostructurality and Synthon Equivalence Between Alcohols and Acids. *Cryst. Growth Des.* **2012**, *12*, 2942–2947. [CrossRef]
89. Reddy, C.M.; Kirchner, M.T.; Gundakaram, R.C.; Padmanabhan, K.A.; Desiraju, G.R. Isostructurality, Polymorphism and Mechanical Properties of Some Hexahalogenated Benzenes: The Nature of Halogen···Halogen Interactions. *Chem.—Eur. J.* **2006**, *12*, 2222–2234. [CrossRef] [PubMed]

90. Asmadi, A.; Kendrick, J.; Leusen, F.J.J. Crystal Structure Prediction and Isostructurality of Three Small Molecules. *Chem.—Eur. J.* **2010**, *16*, 12701–12709. [CrossRef]
91. Owczarzak, A.M.; Kourkoumelis, N.; Hadjikakou, S.K.; Kubicki, M. The impact of the anion size on the crystal packing in 2-mercaptopyrimidine halides; isostructurality and polymorphism. *CrystEngComm* **2013**, *15*, 3607–3614. [CrossRef]
92. Ravat, P.; SeethaLekshmi, S.; Biswas, S.N.; Nandy, P.; Varughese, S. Equivalence of Ethylene and Azo-Bridges in the Modular Design of Molecular Complexes: Role of Weak Interactions. *Cryst. Growth Des.* **2015**, *15*, 2389–2401. [CrossRef]
93. Nath, N.K.; Nangia, A. Isomorphous Crystals by Chloro–Methyl Exchange in Polymorphic Fuchsones. *Cryst. Growth Des.* **2012**, *12*, 5411–5425. [CrossRef]
94. Gonnade, R.G.; Bhadbhade, M.M.; Shashidhar, M.S. Crystal-to-crystal thermal phase transition amongst dimorphs of hexa-O-p-toluoyl-myo-inositol conserving two-dimensional isostructurality. *CrystEngComm* **2010**, *12*, 478–484. [CrossRef]
95. Gelbrich, T.; Hughes, D.S.; Hursthouse, M.B.; Threlfall, T.L. Packing similarity in polymorphs of sulfathiazole. *CrystEngComm* **2008**, *10*, 1328–1334. [CrossRef]
96. Panini, P.; Mohan, T.P.; Gangwar, U.; Sankolli, R.; Chopra, D. Quantitative crystal structure analysis of 1,3,4-thiadiazole derivatives. *CrystEngComm* **2013**, *15*, 4549–4564. [CrossRef]
97. Chopra, D.; Row, T.N.G. Evaluation of the interchangeability of C–H and C–F groups: Insights from crystal packing in a series of isomeric fluorinated benzanilides. *CrystEngComm* **2007**, *10*, 54–67. [CrossRef]
98. Thakuria, R.; Nath, N.K.; Roy, S.; Nangia, A. Polymorphism and isostructurality in sulfonylhydrazones. *CrystEngComm* **2014**, *16*, 4681–4690. [CrossRef]
99. Gelbrich, T.; Hursthouse, M.B. A versatile procedure for the identification, description and quantification of structural similarity in molecular crystals. *CrystEngComm* **2005**, *7*, 324–336. [CrossRef]
100. Dzyabchenko, A.V. Method of crystal-structure similarity searching. *Acta Cryst. Sect. B* **1994**, *50*, 414–425.
101. Suponitsky, K.Y.; Lyssenko, K.A.; Ananyev, I.V.; Kozeev, A.M.; Sheremetev, A.B. Role of Weak Intermolecular Interactions in the Crystal Structure of Tetrakis-furazano[3,4-c:3′,4′-g:3′′,4′′-k:3′′′,4′′′-o] [1,2,5,6,9,10,13,14]octaazacyclohexadecine and Its Solvates. *Cryst. Growth Des.* **2014**, *14*, 4439–4449. [CrossRef]
102. Childs, S.L.; Wood, P.A.; Rodríguez-Hornedo, N.; Reddy, L.S.; Hardcastle, K.I. Analysis of 50 Crystal Structures Containing Carbamazepine Using the Materials Module of Mercury CSD. *Cryst. Growth Des.* **2009**, *9*, 1869–1888. [CrossRef]
103. Gelbrich, T.; Hursthouse, M.B. Systematic investigation of the relationships between 25 crystal structures containing the carbamazepine molecule or a close analogue: A case study of the XPac method. *CrystEngComm* **2006**, *8*, 448–460. [CrossRef]
104. Prohens, R.; Font-Bardia, M.; Barbas, R. Water wires in the nanoporous form II of carbamazepine: A single-crystal X-ray diffraction analysis. *CrystEngComm* **2013**, *15*, 845–847. [CrossRef]
105. Zhong, Z.; Yang, X.; Wang, B.-H.; Yao, Y.-F.; Guo, B.; Yu, L.; Huang, Y.; Xu, J. Solvent-polymer guest exchange in a carbamazepine inclusion complex: Structure, kinetics and implication for guest selection. *CrystEngComm* **2019**, *21*, 2164–2173. [CrossRef]
106. Kennedy, A.R.; Morrison, C.A.; Briggs, N.E.B.; Arbuckle, W. Density and Stability Differences Between Enantiopure and Racemic Salts: Construction and Structural Analysis of a Systematic Series of Crystalline Salt Forms of Methylephedrine. *Cryst. Growth Des.* **2011**, *11*, 1821–1834. [CrossRef]
107. Tumanov, N.A.; Myz, S.A.; Shakhtshneider, T.P.; Boldyreva, E.V. Are meloxicam dimers really the structure-forming units in the 'meloxicam–carboxylic acid' co-crystals family? Relation between crystal structures and dissolution behaviour. *CrystEngComm* **2012**, *14*, 305–313. [CrossRef]
108. Ueto, T.; Takata, N.; Muroyama, N.; Nedu, A.; Sasaki, A.; Tanida, S.; Terada, K. Polymorphs and a Hydrate of Furosemide–Nicotinamide 1:1 Cocrystal. *Cryst. Growth Des.* **2012**, *12*, 485–494. [CrossRef]
109. Galcera, J.; Friščić, T.; Molins, E.; Jones, W. Isostructurality in three-component crystals achieved by the combination of persistent hydrogen bonding motifs and solvent inclusion. *CrystEngComm* **2013**, *15*, 1332–1338. [CrossRef]
110. Briggs, N.E.; Kennedy, A.R.; Morrison, C.A. 42 salt forms of tyramine: Structural comparison and the occurrence of hydrate formation. *Acta Cryst. Sect. B* **2012**, *68*, 453–464. [CrossRef] [PubMed]

111. Salbego, P.R.S.; Bender, C.R.; Hörner, M.; Zanatta, N.; Frizzo, C.P.; Bonacorso, H.G.; Martins, M.A.P. Insights on the Similarity of Supramolecular Structures in Organic Crystals Using Quantitative Indexes. *ACS Omega* **2018**, *3*, 2569–2578. [CrossRef] [PubMed]
112. Surov, A.O.; Simagina, A.A.; Manin, N.G.; Kuzmina, L.G.; Churakov, A.V.; Perlovich, G.L. Fenamate Cocrystals with 4,4′-Bipyridine: Structural and Thermodynamic Aspects. *Cryst. Growth Des.* **2015**, *15*, 228–238. [CrossRef]
113. Sládková, V.; Skalická, T.; Skořepová, E.; Čejka, J.; Eigner, V.; Kratochvíl, B. Systematic solvate screening of trospium chloride: Discovering hydrates of a long-established pharmaceutical. *CrystEngComm* **2015**, *17*, 4712–4721. [CrossRef]
114. Chennuru, R.; Muthudoss, P.; Voguri, R.S.; Ramakrishnan, S.; Vishweshwar, P.; Babu, R.R.C.; Mahapatra, S. Iso-Structurality Induced Solid Phase Transformations: A Case Study with Lenalidomide. *Cryst. Growth Des.* **2017**, *17*, 612–628. [CrossRef]
115. Allen, F.H.; Groom, C.R.; Liebeschuetz, J.W.; Bardwell, D.A.; Olsson, T.S.G.; Wood, P.A. The Hydrogen Bond Environments of 1H-Tetrazole and Tetrazolate Rings: The Structural Basis for Tetrazole–Carboxylic Acid Bioisosterism. *J. Chem. Inf. Model.* **2012**, *52*, 857–866. [CrossRef]
116. Chernyshov, I.Y.; Vener, M.V.; Prikhodchenko, P.V.; Medvedev, A.G.; Lev, O.; Churakov, A.V. Peroxosolvates: Formation Criteria, H2O2 Hydrogen Bonding, and Isomorphism with the Corresponding Hydrates. *Cryst. Growth Des.* **2017**, *17*, 214–220. [CrossRef]
117. Cummings, M.D.; Sekharan, S. Structure-Based Macrocycle Design in Small-Molecule Drug Discovery and Simple Metrics to Identify Opportunities for Macrocyclization of Small-Molecule Ligands. *J. Med. Chem.* **2019**, *62*, 6843–6853. [CrossRef] [PubMed]
118. Gavezzotti, A. Are Crystal Structures Predictable? *Acc. Chem. Res.* **1994**, *27*, 309–314. [CrossRef]
119. Gavezzotti, A. The Crystal Packing of Organic Molecules: Challenge and Fascination Below 1000 Da. *Crystallogr. Rev.* **1998**, *7*, 5–121. [CrossRef]
120. Chemla, D.S.; Zyss, J. *Nonlinear Optical Properties of Organic Molecules and Crystals*; Elsevier: Amsterdam, The Netherlands, 1987.
121. Ostroverkhova, O. Organic Optoelectronic Materials: Mechanisms and Applications. *Chem. Rev.* **2016**, *116*, 13279–13412. [CrossRef] [PubMed]
122. Tyagi, N.; Sinha, N.; Yadav, H.; Kumar, B. Growth, morphology, structure and characterization of l-histidinium dihydrogen arsenate orthoarsenic acid single crystal. *Acta Cryst. Sect. B* **2016**, *72*, 593–601. [CrossRef] [PubMed]
123. Gao, Z.; Tian, X.; Zhang, J.; Wu, Q.; Lu, Q.; Tao, X. Large-Sized Crystal Growth and Electric-Elastic Properties of α-$BaTeMo_2O_9$ Single Crystal. *Cryst. Growth Des.* **2015**, *15*, 759–763. [CrossRef]
124. Chen, F.; Jiang, C.; Tian, S.; Yu, F.; Cheng, X.; Duan, X.; Wang, Z.; Zhao, X. Electroelastic Features of Piezoelectric $Bi_2ZnB_2O_7$ Crystal. *Cryst. Growth Des.* **2018**, *18*, 3988–3996. [CrossRef]
125. Leclaire, N.A.; Li, M.; Véron, A.C.; Neels, A.; Heier, J.; Reimers, J.R.; Nüesch, F.A. Cyanine platelet single crystals: Growth, crystal structure and optical spectra. *Phys. Chem. Chem. Phys.* **2018**, *20*, 29166–29173. [CrossRef]
126. Ozdemir, R.; Park, S.; Deneme, İ.; Park, Y.; Zorlu, Y.; Ardic Alidagi, H.; Harmandar, K.; Kim, C.; Usta, H. Triisopropylsilylethynyl-substituted indenofluorenes: Carbonyl versus dicyanovinylene functionalization in one-dimensional molecular crystals and solution-processed n-channel OFETs. *Org. Chem. Front.* **2018**, *5*, 2912–2924. [CrossRef]
127. Glöcklhofer, F.; Morawietz, A.J.; Stöger, B.; Unterlass, M.M.; Fröhlich, J. Extending the Scope of a New Cyanation: Design and Synthesis of an Anthracene Derivative with an Exceptionally Low LUMO Level and Improved Solubility. *ACS Omega* **2017**, *2*, 1594–1600. [CrossRef] [PubMed]
128. Wang, C.; Dong, H.; Jiang, L.; Hu, W. Organic semiconductor crystals. *Chem. Soc. Rev.* **2018**, *47*, 422–500. [CrossRef] [PubMed]
129. Stevens, J.S.; Walczak, M.; Jaye, C.; Fischer, D.A. In Situ Solid-State Reactions Monitored by X-ray Absorption Spectroscopy: Temperature-Induced Proton Transfer Leads to Chemical Shifts. *Chem.—Eur. J.* **2016**, *22*, 15600–15604. [CrossRef] [PubMed]
130. Liu, G.; Liu, J.; Liu, Y.; Tao, X. Oriented Single-Crystal-to-Single-Crystal Phase Transition with Dramatic Changes in the Dimensions of Crystals. *J. Am. Chem. Soc.* **2014**, *136*, 590–593. [CrossRef] [PubMed]

131. Chou, C.-M.; Nobusue, S.; Saito, S.; Inoue, D.; Hashizume, D.; Yamaguchi, S. Highly bent crystals formed by restrained π-stacked columns connected via alkylene linkers with variable conformations. *Chem. Sci.* **2015**, *6*, 2354–2359. [CrossRef] [PubMed]
132. Commins, P.; Desta, I.T.; Karothu, D.P.; Panda, M.K.; Naumov, P. Crystals on the move: Mechanical effects in dynamic solids. *Chem. Commun.* **2016**, *52*, 13941–13954. [CrossRef] [PubMed]
133. Boldyreva, E.V. High-pressure diffraction studies of molecular organic solids. A personal view. *Acta Cryst. Sect. A* **2008**, *64*, 218–231. [CrossRef]
134. Bull, C.L.; Flowitt-Hill, G.; de Gironcoli, S.; Küçükbenli, E.; Parsons, S.; Pham, C.H.; Playford, H.Y.; Tucker, M.G. ζ-Glycine: Insight into the mechanism of a polymorphic phase transition. *IUCrJ* **2017**, *4*, 569–574. [CrossRef]
135. Giordano, N.; Beavers, C.M.; Kamenev, K.V.; Marshall, W.G.; Moggach, S.A.; Patterson, S.D.; Teat, S.J.; Warren, J.E.; Wood, P.A.; Parsons, S. High-pressure polymorphism in L-threonine between ambient pressure and 22 GPa. *CrystEngComm* **2019**, *21*, 4444–4456. [CrossRef]
136. Sun, C.; Grant, D.J.W. Influence of Crystal Shape on the Tableting Performance of L-Lysine Monohydrochloride Dihydrate. *J. Pharm. Sci.* **2001**, *90*, 569–579. [CrossRef]
137. Rosbottom, I.; Ma, C.Y.; Turner, T.D.; O'Connell, R.A.; Loughrey, J.; Sadiq, G.; Davey, R.J.; Roberts, K.J. Influence of Solvent Composition on the Crystal Morphology and Structure of p-Aminobenzoic Acid Crystallized from Mixed Ethanol and Nitromethane Solutions. *Cryst. Growth Des.* **2017**, *17*, 4151–4161. [CrossRef]
138. Zhao, P.; Liu, X.; Wang, L.; Gao, Z.; Yang, Y.; Hao, H.; Xie, C.; Bao, Y. Predicting the crystal habit of photoinitiator XBPO and elucidating the solvent effect on crystal faces. *CrystEngComm* **2019**, *21*, 2422–2430. [CrossRef]
139. O'Mahony, M.; Seaton, C.C.; Croker, D.M.; Veesler, S.; Rasmuson, Å.C.; Hodnett, B.K. Investigating the dissolution of the metastable triclinic polymorph of carbamazepine using in situ microscopy. *CrystEngComm* **2014**, *16*, 4133–4141. [CrossRef]
140. Vologzhanina, A.V.; Belov, A.S.; Novikov, V.V.; Dolganov, A.V.; Romanenko, G.V.; Ovcharenko, V.I.; Korlyukov, A.A.; Buzin, M.I.; Voloshin, Y.Z. Synthesis and Temperature-Induced Structural Phase and Spin Transitions in Hexadecylboron-Capped Cobalt(II) Hexachloroclathrochelate and Its Diamagnetic Iron(II)-Encapsulating Analogue. *Inorg. Chem.* **2015**, *54*, 5827–5838. [CrossRef] [PubMed]
141. Pavlov, A.A.; Nelyubina, Y.V.; Kats, S.V.; Penkova, L.V.; Efimov, N.N.; Dmitrienko, A.O.; Vologzhanina, A.V.; Belov, A.S.; Voloshin, Y.Z.; Novikov, V.V. Polymorphism in a Cobalt-Based Single-Ion Magnet Tuning Its Barrier to Magnetization Relaxation. *J. Phys. Chem. Lett.* **2016**, *7*, 4111–4116. [CrossRef] [PubMed]
142. Nguyen, T.T.H.; Rosbottom, I.; Marziano, I.; Hammond, R.B.; Roberts, K.J. Crystal Morphology and Interfacial Stability of RS-Ibuprofen in Relation to Its Molecular and Synthonic Structure. *Cryst. Growth Des.* **2017**, *17*, 3088–3099. [CrossRef]
143. Rosbottom, I.; Pickering, J.H.; Etbon, B.; Hammond, R.B.; Roberts, K.J. Examination of inequivalent wetting on the crystal habit surfaces of RS-ibuprofen using grid-based molecular modelling. *Phys. Chem. Chem. Phys.* **2018**, *20*, 11622–11633. [CrossRef]
144. Turner, T.D.; Hatcher, L.E.; Wilson, C.C.; Roberts, K.J. Habit Modification of the Active Pharmaceutical Ingredient Lovastatin Through a Predictive Solvent Selection Approach. *J. Pharm. Sci.* **2019**, *108*, 1779–1787. [CrossRef]
145. Gajda, R.; Domański, M.A.; Malinska, M.; Makal, A. Crystal morphology fixed by interplay of π-stacking and hydrogen bonds – the case of 1-hydroxypyrene. *CrystEngComm* **2019**, *21*, 1701–1717. [CrossRef]
146. Han, D.; Karmakar, T.; Bjelobrk, Z.; Gong, J.; Parrinello, M. Solvent-mediated morphology selection of the active pharmaceutical ingredient isoniazid: Experimental and simulation studies. *Chem. Eng. Sci.* **2019**, *204*, 320–328. [CrossRef]
147. Destri, G.L.; Marrazzo, A.; Rescifina, A.; Punzo, F. Crystal Morphologies and Polymorphs in Tolbutamide Microcrystalline Powder. *J. Pharm. Sci.* **2013**, *102*, 73–83. [CrossRef]
148. Thirupugalmani, K.; Venkatesh, M.; Karthick, S.; Maurya, K.K.; Vijayan, N.; Chaudhary, A.K.; Brahadeeswaran, S. Influence of polar solvents on growth of potentially NLO active organic single crystals of N-benzyl-2-methyl-4-nitroaniline and their efficiency in terahertz generation. *CrystEngComm* **2017**, *19*, 2623–2631. [CrossRef]

149. Croker, D.M.; Kelly, D.M.; Horgan, D.E.; Hodnett, B.K.; Lawrence, S.E.; Moynihan, H.A.; Rasmuson, Å.C. Demonstrating the Influence of Solvent Choice and Crystallization Conditions on Phenacetin Crystal Habit and Particle Size Distribution. *Org. Process Res. Dev.* **2015**, *19*, 1826–1836. [CrossRef]
150. Poornachary, S.K.; Lau, G.; Chow, P.S.; Tan, R.B.H.; George, N. The Effect and Counter-Effect of Impurities on Crystallization of an Agrochemical Active Ingredient: Stereochemical Rationalization and Nanoscale Crystal Growth Visualization. *Cryst. Growth Des.* **2011**, *11*, 492–500. [CrossRef]
151. Anuar, N.; Wan Daud, W.R.; Roberts, K.J.; Kamarudin, S.K.; Tasirin, S.M. Morphology and Associated Surface Chemistry of l-Isoleucine Crystals Modeled under the Influence of l-Leucine Additive Molecules. *Cryst. Growth Des.* **2012**, *12*, 2195–2203. [CrossRef]
152. Tang, Y.; Gao, J. Investigation of the Effects of Sodium Dicarboxylates on the Crystal Habit of Calcium Sulfate α-Hemihydrate. *Langmuir* **2017**, *33*, 9637–9644. [CrossRef]
153. Schmidt, C.; Jones, M.J.; Ulrich, J. The Influence of Additives and Impurities on Crystallization. In *Crystallization*; John Wiley & Sons, Ltd.: Hoboken, NJ, USA, 2013; pp. 105–127.
154. Liu, D.; Liu, Y.; Dai, F.; Zhao, J.; Yang, K.; Liu, C. Size- and morphology-controllable synthesis of MIL-96 (Al) by hydrolysis and coordination modulation of dual aluminium source and ligand systems. *Dalton Trans.* **2015**, *44*, 16421–16429. [CrossRef]
155. Liu, D.; Yan, L.; Li, L.; Gu, X.; Dai, P.; Yang, L.; Liu, Y.; Liu, C.; Zhao, G.; Zhao, X. Impact of moderative ligand hydrolysis on morphology evolution and the morphology-dependent breathing effect performance of MIL-53(Al). *CrystEngComm* **2018**, *20*, 2102–2111. [CrossRef]
156. Zelinskii, G.E.; Belov, A.S.; Lebed, E.G.; Vologzhanina, A.V.; Novikov, V.V.; Voloshin, Y.Z. Synthesis, structure and reactivity of iron(II) clathrochelates with terminal formyl (acetal) groups. *Inorg. Chim. Acta* **2016**, *440*, 154–164. [CrossRef]
157. Koradia, V.; de Diego, H.L.; Elema, M.R.; Rantanen, J. Integrated Approach to Study the Dehydration Kinetics of Nitrofurantoin Monohydrate. *J. Pharm. Sci.* **2010**, *99*, 3966–3976. [CrossRef]
158. Thakuria, R.; Eddleston, M.D.; Chow, E.H.H.; Lloyd, G.O.; Aldous, B.J.; Krzyzaniak, J.F.; Bond, A.D.; Jones, W. Use of in Situ Atomic Force Microscopy to Follow Phase Changes at Crystal Surfaces in Real Time. *Angew. Chem. Int. Ed.* **2013**, *52*, 10541–10544. [CrossRef]
159. Park, Y.; Boerrigter, S.X.M.; Yeon, J.; Lee, S.H.; Kang, S.K.; Lee, E.H. New Metastable Packing Polymorph of Donepezil Grown on Stable Polymorph Substrates. *Cryst. Growth Des.* **2016**, *16*, 2552–2560. [CrossRef]
160. Bond, A.D.; Boese, R.; Desiraju, G.R. On the Polymorphism of Aspirin: Crystalline Aspirin as Intergrowths of Two "Polymorphic" Domains. *Angew. Chem. Int. Ed.* **2007**, *46*, 618–622. [CrossRef]
161. Mishra, M.K.; Desiraju, G.R.; Ramamurty, U.; Bond, A.D. Studying Microstructure in Molecular Crystals with Nanoindentation: Intergrowth Polymorphism in Felodipine. *Angew. Chem. Int. Ed.* **2014**, *53*, 13102–13105. [CrossRef]
162. Croker, D.M.; Davey, R.J.; Rasmuson, Å.C.; Seaton, C.C. Solution mediated phase transformations between co-crystals. *CrystEngComm* **2013**, *15*, 2044–2047. [CrossRef]
163. Bhandary, S.; Chopra, D. Silicone Oil Induced Spontaneous Single-Crystal-to-Single-Crystal Phase Transitions in Ethynyl Substituted ortho- and meta-Fluorinated Benzamides. *Cryst. Growth Des.* **2017**, *17*, 4533–4540. [CrossRef]
164. Ravi, A.; Sureshan, K.M. Tunable Mechanical Response from a Crystal Undergoing Topochemical Dimerization: Instant Explosion at a Faster Rate and Chemical Storage of a Harvestable Explosion at a Slower Rate. *Angew. Chem. Int. Ed.* **2018**, *57*, 9362–9366. [CrossRef]
165. Lee, A.Y.; Ulman, A.; Myerson, A.S. Crystallization of Amino Acids on Self-Assembled Monolayers of Rigid Thiols on Gold. *Langmuir* **2002**, *18*, 5886–5898. [CrossRef]
166. Cox, J.R.; Dabros, M.; Shaffer, J.A.; Thalladi, V.R. Selective Crystal Growth of the Anhydrous and Monohydrate Forms of Theophylline on Self-Assembled Monolayers. *Angew. Chem. Int. Ed.* **2007**, *46*, 1988–1991. [CrossRef]
167. Urbelis, J.H.; Swift, J.A. Phase-Selective Crystallization of Perylene on Monolayer Templates. *Cryst. Growth Des.* **2014**, *14*, 5244–5251. [CrossRef]
168. Zhang, J.; Liu, A.; Han, Y.; Ren, Y.; Gong, J.; Li, W.; Wang, J. Effects of Self-Assembled Monolayers on Selective Crystallization of Tolbutamide. *Cryst. Growth Des.* **2011**, *11*, 5498–5506. [CrossRef]
169. Solomos, M.A.; Capacci-Daniel, C.; Rubinson, J.F.; Swift, J.A. Polymorph Selection via Sublimation onto Siloxane Templates. *Cryst. Growth Des.* **2018**, *18*, 6965–6972. [CrossRef]

170. Serrano, D.R.; Mugheirbi, N.A.; O'Connell, P.; Leddy, N.; Healy, A.M.; Tajber, L. Impact of Substrate Properties on the Formation of Spherulitic Films: A Case Study of Salbutamol Sulfate. *Cryst. Growth Des.* **2016**, *16*, 3853–3858. [CrossRef]
171. Patel, M.A.; Nguyen, B.; Chadwick, K. Predicting the Nucleation Induction Time Based on Preferred Intermolecular Interactions. *Cryst. Growth Des.* **2017**, *17*, 4613–4621. [CrossRef]
172. Telford, R.; Seaton, C.C.; Clout, A.; Buanz, A.; Gaisford, S.; Williams, G.R.; Prior, T.J.; Okoye, C.H.; Munshi, T.; Scowen, I.J. Stabilisation of metastable polymorphs: The case of paracetamol form III. *Chem. Commun.* **2016**, *52*, 12028–12031. [CrossRef]
173. Zhang, K.; Xu, S.; Liu, S.; Tang, W.; Fu, X.; Gong, J. Novel Strategy to Control Polymorph Nucleation of Gamma Pyrazinamide by Preferred Intermolecular Interactions during Heterogeneous Nucleation. *Cryst. Growth Des.* **2018**, *18*, 4874–4879. [CrossRef]
174. Rao, K.P.; Higuchi, M.; Sumida, K.; Furukawa, S.; Duan, J.; Kitagawa, S. Design of Superhydrophobic Porous Coordination Polymers through the Introduction of External Surface Corrugation by the Use of an Aromatic Hydrocarbon Building Unit. *Angew. Chem. Int. Ed.* **2014**, *53*, 8225–8230. [CrossRef]
175. Zhang, J.; Mitchell, L.A.; Parrish, D.A.; Shreeve, J.M. Enforced Layer-by-Layer Stacking of Energetic Salts towards High-Performance Insensitive Energetic Materials. *J. Am. Chem. Soc.* **2015**, *137*, 10532–10535. [CrossRef]
176. Wang, K.; Mishra, M.K.; Sun, C.C. Exceptionally Elastic Single-Component Pharmaceutical Crystals. *Chem. Mater.* **2019**, *31*, 1794–1799. [CrossRef]
177. Devarapalli, R.; Kadambi, S.B.; Chen, C.-T.; Krishna, G.R.; Kammari, B.R.; Buehler, M.J.; Ramamurty, U.; Reddy, C.M. Remarkably Distinct Mechanical Flexibility in Three Structurally Similar Semiconducting Organic Crystals Studied by Nanoindentation and Molecular Dynamics. *Chem. Mater.* **2019**, *31*, 1391–1402. [CrossRef]
178. SeethaLekshmi, S.; Kiran, M.S.R.N.; Ramamurty, U.; Varughese, S. Molecular Basis for the Mechanical Response of Sulfa Drug Crystals. *Chem.—Eur. J.* **2019**, *25*, 526–537. [CrossRef] [PubMed]
179. Krishna, G.R.; Shi, L.; Bag, P.P.; Sun, C.C.; Reddy, C.M. Correlation Among Crystal Structure, Mechanical Behavior, and Tabletability in the Co-Crystals of Vanillin Isomers. *Cryst. Growth Des.* **2015**, *15*, 1827–1832. [CrossRef]
180. Zolotarev, P.N.; Moret, M.; Rizzato, S.; Proserpio, D.M. Searching New Crystalline Substrates for OMBE: Topological and Energetic Aspects of Cleavable Organic Crystals. *Cryst. Growth Des.* **2016**, *16*, 1572–1582. [CrossRef]
181. Reddy, C.M.; Gundakaram, R.C.; Basavoju, S.; Kirchner, M.T.; Padmanabhan, K.A.; Desiraju, G.R. Structural basis for bending of organic crystals. *Chem. Commun.* **2005**, 3945–3947. [CrossRef] [PubMed]
182. Chattoraj, S.; Shi, L.; Sun, C.C. Understanding the relationship between crystal structure, plasticity and compaction behaviour of theophylline, methyl gallate, and their 1:1 co-crystal. *CrystEngComm* **2010**, *12*, 2466–2472. [CrossRef]
183. Veits, G.K.; Carter, K.K.; Cox, S.J.; McNeil, A.J. Developing a Gel-Based Sensor Using Crystal Morphology Prediction. *J. Am. Chem. Soc.* **2016**, *138*, 12228–12233. [CrossRef] [PubMed]
184. Bučar, D.-K.; Lancaster, R.W.; Bernstein, J. Disappearing Polymorphs Revisited. *Angew. Chem. Int. Ed.* **2015**, *54*, 6972–6993. [CrossRef] [PubMed]
185. Galek, P.T.A.; Allen, F.H.; Fábián, L.; Feeder, N. Knowledge-based H-bond prediction to aid experimental polymorph screening. *CrystEngComm* **2009**, *11*, 2634–2639. [CrossRef]
186. Galek, P.T.A.; Fábián, L.; Motherwell, W.D.S.; Allen, F.H.; Feeder, N. Knowledge-based model of hydrogen-bonding propensity in organic crystals. *Acta Cryst. Sect. B* **2007**, *63*, 768–782. [CrossRef]
187. Galek, P.T.A.; Chisholm, J.A.; Pidcock, E.; Wood, P.A. Hydrogen-bond coordination in organic crystal structures: Statistics, predictions and applications. *Acta Cryst. Sect. B* **2014**, *70*, 91–105. [CrossRef]
188. Galek, P.T.A.; Pidcock, E.; Wood, P.A.; Bruno, I.J.; Groom, C.R. One in half a million: A solid form informatics study of a pharmaceutical crystal structure. *CrystEngComm* **2012**, *14*, 2391–2403. [CrossRef]
189. Abramov, Y.A. Current Computational Approaches to Support Pharmaceutical Solid Form Selection. *Org. Process Res. Dev.* **2013**, *17*, 472–485. [CrossRef]
190. Feeder, N.; Pidcock, E.; Reilly, A.M.; Sadiq, G.; Doherty, C.L.; Back, K.R.; Meenan, P.; Docherty, R. The integration of solid-form informatics into solid-form selection. *J. Pharm. Pharm.* **2015**, *67*, 857–868. [CrossRef] [PubMed]

191. Allen, F.H.; Wood, P.A.; Galek, P.T.A. The versatile role of the ethynyl group in crystal packing: An interaction propensity study. *Acta Cryst. Sect. B* **2013**, *69*, 281–287. [CrossRef] [PubMed]
192. Allen, F.H.; Wood, P.A.; Galek, P.T.A. Role of chloroform and dichloromethane solvent molecules in crystal packing: An interaction propensity study. *Acta Cryst. Sect. B* **2013**, *69*, 379–388. [CrossRef] [PubMed]
193. Srirambhatla, V.K.; Kraft, A.; Watt, S.; Powell, A.V. Crystal Design Approaches for the Synthesis of Paracetamol Co-Crystals. *Cryst. Growth Des.* **2012**, *12*, 4870–4879. [CrossRef]
194. Vologzhanina, A.V.; Sokolov, A.V.; Purygin, P.P.; Zolotarev, P.N.; Blatov, V.A. Knowledge-Based Approaches to H-Bonding Patterns in Heterocycle-1-Carbohydrazoneamides. *Cryst. Growth Des.* **2016**, *16*, 6354–6362. [CrossRef]
195. Hulme, A.T.; Johnston, A.; Florence, A.J.; Fernandes, P.; Shankland, K.; Bedford, C.T.; Welch, G.W.A.; Sadiq, G.; Haynes, D.A.; Motherwell, W.D.S.; et al. Search for a Predicted Hydrogen Bonding Motif—A Multidisciplinary Investigation into the Polymorphism of 3-Azabicyclo[3.3.1]nonane-2,4-dione. *J. Am. Chem. Soc.* **2007**, *129*, 3649–3657. [CrossRef] [PubMed]
196. Nauha, E.; Bernstein, J. "Predicting" Polymorphs of Pharmaceuticals Using Hydrogen Bond Propensities: Probenecid and Its Two Single-Crystal-to-Single-Crystal Phase Transitions. *J. Pharm. Sci.* **2015**, *104*, 2056–2061. [CrossRef]
197. Nauha, E.; Bernstein, J. "Predicting" Crystal Forms of Pharmaceuticals Using Hydrogen Bond Propensities: Two Test Cases. *Cryst. Growth Des.* **2014**, *14*, 4364–4370. [CrossRef]
198. Jones, W.; Motherwell, W.D.S.; Trask, A.V. Pharmaceutical Cocrystals: An Emerging Approach to Physical Property Enhancement. *MRS Bull.* **2006**, *31*, 875–879. [CrossRef]
199. Sathisaran, I.; Dalvi, S.V. Engineering Cocrystals of Poorly Water-Soluble Drugs to Enhance Dissolution in Aqueous Medium. *Pharmaceutics* **2018**, *10*, 108. [CrossRef] [PubMed]
200. Schultheiss, N.; Newman, A. Pharmaceutical Cocrystals and Their Physicochemical Properties. *Cryst. Growth Des.* **2009**, *9*, 2950–2967. [CrossRef] [PubMed]
201. Karki, S.; Friščić, T.; Fábián, L.; Laity, P.R.; Day, G.M.; Jones, W. Improving Mechanical Properties of Crystalline Solids by Cocrystal Formation: New Compressible Forms of Paracetamol. *Adv. Mater.* **2009**, *21*, 3905–3909. [CrossRef]
202. Saha, S.; Desiraju, G.R. Acid···Amide Supramolecular Synthon in Cocrystals: From Spectroscopic Detection to Property Engineering. *J. Am. Chem. Soc.* **2018**, *140*, 6361–6373. [CrossRef] [PubMed]
203. Zhang, J.; Shreeve, J.M. Time for pairing: Cocrystals as advanced energetic materials. *CrystEngComm* **2016**, *18*, 6124–6133. [CrossRef]
204. Bolton, O.; Simke, L.R.; Pagoria, P.F.; Matzger, A.J. High Power Explosive with Good Sensitivity: A 2:1 Cocrystal of CL-20: HMX. *Cryst. Growth Des.* **2012**, *12*, 4311–4314. [CrossRef]
205. Gryl, M.; Seidler, T.; Stadnicka, K.; Matulková, I.; Němec, I.; Tesařová, N.; Němec, P. The crystal structure and optical properties of a pharmaceutical co-crystal—The case of the melamine–barbital addition compound. *CrystEngComm* **2014**, *16*, 5765–5768. [CrossRef]
206. Christopherson, J.-C.; Topić, F.; Barrett, C.J.; Friščić, T. Halogen-Bonded Cocrystals as Optical Materials: Next-Generation Control over Light–Matter Interactions. *Cryst. Growth Des.* **2018**, *18*, 1245–1259. [CrossRef]
207. Noa, F.M.A.; Mehlana, G. Co-crystals and salts of vanillic acid and vanillin with amines. *CrystEngComm* **2018**, *20*, 896–905.
208. Walsh, R.D.B.; Bradner, M.W.; Fleischman, S.; Morales, L.A.; Moulton, B.; Rodríguez-Hornedo, N.; Zaworotko, M.J. Crystal engineering of the composition of pharmaceutical phases. *Chem. Commun.* **2003**, 186–187. [CrossRef] [PubMed]
209. Price(Sally), S.L. Computed Crystal Energy Landscapes for Understanding and Predicting Organic Crystal Structures and Polymorphism. *Acc. Chem. Res.* **2009**, *42*, 117–126.
210. Etter, M.C. Encoding and decoding hydrogen-bond patterns of organic compounds. *Acc. Chem. Res.* **1990**, *23*, 120–126. [CrossRef]
211. Delori, A.; Galek, P.T.A.; Pidcock, E.; Jones, W. Quantifying Homo- and Heteromolecular Hydrogen Bonds as a Guide for Adduct Formation. *Chem. Eur. J.* **2012**, *18*, 6835–6846. [CrossRef] [PubMed]
212. Delori, A.; Galek, P.T.A.; Pidcock, E.; Patni, M.; Jones, W. Knowledge-based hydrogen bond prediction and the synthesis of salts and cocrystals of the anti-malarial drug pyrimethamine with various drug and GRAS molecules. *CrystEngComm* **2013**, *15*, 2916–2928. [CrossRef]

213. Bhogala, B.R.; Basavoju, S.; Nangia, A. Tape and layer structures in cocrystals of some di- and tricarboxylic acids with 4,4′-bipyridines and isonicotinamide. From binary to ternary cocrystals. *CrystEngComm* **2005**, *7*, 551–562. [CrossRef]
214. Cruz-Cabeza, A.J. Acid–base crystalline complexes and the pKa rule. *CrystEngComm* **2012**, *14*, 6362–6365. [CrossRef]
215. Chamorro Orué, A.I.; Boese, R.; Schauerte, C.; Merz, K. An Experimental and Theoretical Approach to Control Salt vs Cocrystal vs Hybrid Formation—Crystal Engineering of an E/Z-Butenedioic Acid/Phthalazine System. *Cryst. Growth Des.* **2019**, *19*, 1616–1620. [CrossRef]
216. Sandhu, B.; McLean, A.; Sinha, A.S.; Desper, J.; Sarjeant, A.A.; Vyas, S.; Reutzel-Edens, S.M.; Aakeröy, C.B. Evaluating Competing Intermolecular Interactions through Molecular Electrostatic Potentials and Hydrogen-Bond Propensities. *Cryst. Growth Des.* **2018**, *18*, 466–478. [CrossRef]
217. Wang, J.-R.; Ye, C.; Mei, X. Structural and physicochemical aspects of hydrochlorothiazide co-crystals. *CrystEngComm* **2014**, *16*, 6996–7003. [CrossRef]
218. Eddleston, M.D.; Arhangelskis, M.; Fábián, L.; Tizzard, G.J.; Coles, S.J.; Jones, W. Investigation of an Amide-Pseudo Amide Hydrogen Bonding Motif within a Series of Theophylline: Amide Cocrystals. *Cryst. Growth Des.* **2016**, *16*, 51–58. [CrossRef]
219. Corpinot, M.K.; Stratford, S.A.; Arhangelskis, M.; Anka-Lufford, J.; Halasz, I.; Judaš, N.; Jones, W.; Bučar, D.-K. On the predictability of supramolecular interactions in molecular cocrystals—the view from the bench. *CrystEngComm* **2016**, *18*, 5434–5439. [CrossRef]
220. Wang, T.; Stevens, J.S.; Vetter, T.; Whitehead, G.F.S.; Vitorica-Yrezabal, I.J.; Hao, H.; Cruz-Cabeza, A.J. Salts, Cocrystals, and Ionic Cocrystals of a "Simple" Tautomeric Compound. *Cryst. Growth Des.* **2018**, *18*, 6973–6983. [CrossRef]
221. Mapp, L.K.; Coles, S.J.; Aitipamula, S. Design of Cocrystals for Molecules with Limited Hydrogen Bonding Functionalities: Propyphenazone as a Model System. *Cryst. Growth Des.* **2017**, *17*, 163–174. [CrossRef]
222. Liu, F.; Song, Y.; Liu, Y.-N.; Li, Y.-T.; Wu, Z.-Y.; Yan, C.-W. Drug-Bridge-Drug Ternary Cocrystallization Strategy for Antituberculosis Drugs Combination. *Cryst. Growth Des.* **2018**, *18*, 1283–1286. [CrossRef]
223. Almansa, C.; Mercè, R.; Tesson, N.; Farran, J.; Tomàs, J.; Plata-Salamán, C.R. Co-crystal of Tramadol Hydrochloride–Celecoxib (ctc): A Novel API–API Co-crystal for the Treatment of Pain. *Cryst. Growth Des.* **2017**, *17*, 1884–1892. [CrossRef]
224. Skořepová, E.; Hušák, M.; Čejka, J.; Zámostný, P.; Kratochvíl, B. Increasing dissolution of trospium chloride by co-crystallization with urea. *J. Cryst. Growth* **2014**, *399*, 19–26. [CrossRef]
225. Chandra, A.; Ghate, M.V.; Aithal, K.S.; Lewis, S.A. In silico prediction coupled with in vitro experiments and absorption modeling to study the inclusion complex of telmisartan with modified beta-cyclodextrin. *J. Incl. Phenom. Macrocycl. Chem.* **2018**, *91*, 47–60. [CrossRef]
226. Tothadi, S.; Desiraju, G.R. Designing ternary cocrystals with hydrogen bonds and halogen bonds. *Chem. Commun.* **2013**, *49*, 7791–7793. [CrossRef]
227. Arman, H.D.; Gieseking, R.L.; Hanks, T.W.; Pennington, W.T. Complementary halogen and hydrogen bonding: Sulfur···iodine interactions and thioamide ribbons. *Chem. Commun.* **2010**, *46*, 1854–1856. [CrossRef]
228. Topić, F.; Rissanen, K. Systematic Construction of Ternary Cocrystals by Orthogonal and Robust Hydrogen and Halogen Bonds. *J. Am. Chem. Soc.* **2016**, *138*, 6610–6616. [CrossRef] [PubMed]
229. Seaton, C.C.; Blagden, N.; Munshi, T.; Scowen, I.J. Creation of Ternary Multicomponent Crystals by Exploitation of Charge-Transfer Interactions. *Chem.—Eur. J.* **2013**, *19*, 10663–10671. [CrossRef] [PubMed]
230. Thomas, L.H.; Blagden, N.; Gutmann, M.J.; Kallay, A.A.; Parkin, A.; Seaton, C.C.; Wilson, C.C. Tuning Proton Behavior in a Ternary Molecular Complex. *Cryst. Growth Des.* **2010**, *10*, 2770–2774. [CrossRef]
231. Mishra, M.K.; Mukherjee, A.; Ramamurty, U.; Desiraju, G.R. Crystal chemistry and photomechanical behavior of 3,4-dimethoxycinnamic acid: Correlation between maximum yield in the solid-state topochemical reaction and cooperative molecular motion. *IUCrJ* **2015**, *2*, 653–660. [CrossRef] [PubMed]
232. Mir, N.A.; Dubey, R.; Desiraju, G.R. Four- and five-component molecular solids: Crystal engineering strategies based on structural inequivalence. *IUCrJ* **2016**, *3*, 96–101. [CrossRef] [PubMed]
233. Paul, M.; Chakraborty, S.; Desiraju, G.R. Six-Component Molecular Solids: $ABC[D_{1-(x+y)}E_xF_y]_2$. *J. Am. Chem. Soc.* **2018**, *140*, 2309–2315. [CrossRef]

234. Sander, J.R.G.; Bučar, D.-K.; Henry, R.F.; Giangiorgi, B.N.; Zhang, G.G.Z.; MacGillivray, L.R. 'Masked synthons' in crystal engineering: Insulated components in acetaminophen cocrystal hydrates. *CrystEngComm* **2013**, *15*, 4816–4822. [CrossRef]
235. Oswald, I.D.H.; Allan, D.R.; McGregor, P.A.; Motherwell, W.D.S.; Parsons, S.; Pulham, C.R. The formation of paracetamol (acetaminophen) adducts with hydrogen-bond acceptors. *Acta Cryst. Sect. B* **2002**, *58*, 1057–1066. [CrossRef]
236. Oswald, I.D.H.; Motherwell, W.D.S.; Parsons, S.; Pidcock, E.; Pulham, C.R. Rationalisation of Co-Crystal Formation Through Knowledge-Mining. *Crystallogr. Rev.* **2004**, *10*, 57–66. [CrossRef]
237. Wicker, J.G.P.; Crowley, L.M.; Robshaw, O.; Little, E.J.; Stokes, S.P.; Cooper, R.I.; Lawrence, S.E. Will they co-crystallize? *CrystEngComm* **2017**, *19*, 5336–5340. [CrossRef]
238. Fábián, L. Cambridge Structural Database Analysis of Molecular Complementarity in Cocrystals. *Cryst. Growth Des.* **2009**, *9*, 1436–1443. [CrossRef]
239. Surov, A.O.; Churakov, A.V.; Proshin, A.N.; Dai, X.-L.; Lu, T.; Perlovich, G.L. Cocrystals of a 1,2,4-thiadiazole-based potent neuroprotector with gallic acid: Solubility, thermodynamic stability relationships and formation pathways. *Phys. Chem. Chem. Phys.* **2018**, *20*, 14469–14481. [CrossRef] [PubMed]
240. Karki, S.; Friščić, T.; Fábián, L.; Jones, W. New solid forms of artemisinin obtained through cocrystallisation. *CrystEngComm* **2010**, *12*, 4038–4041. [CrossRef]
241. Alsubaie, M.; Aljohani, M.; Erxleben, A.; McArdle, P. Cocrystal Forms of the BCS Class IV Drug Sulfamethoxazole. *Cryst. Growth Des.* **2018**, *18*, 3902–3912. [CrossRef]
242. Cadden, J.; Klooster, W.T.; Coles, S.J.; Aitipamula, S. Cocrystals of Leflunomide: Design, Structural, and Physicochemical Evaluation. *Cryst. Growth Des.* **2019**, *19*, 3923–3933. [CrossRef]
243. Gryl, M.; Rydz, A.; Wojnarska, J.; Krawczuk, A.; Kozieł, M.; Seidler, T.; Ostrowska, K.; Marzec, M.; Stadnicka, K.M. Origin of chromic effects and crystal-to-crystal phase transition in the polymorphs of tyraminium violurate. *IUCrJ* **2019**, *6*, 226–237. [CrossRef] [PubMed]
244. Robertson, C.C.; Wright, J.S.; Carrington, E.J.; Perutz, R.N.; Hunter, C.A.; Brammer, L. Hydrogen bonding vs. halogen bonding: The solvent decides. *Chem. Sci.* **2017**, *8*, 5392–5398. [CrossRef]
245. Wood, P.A.; Olsson, T.S.G.; Cole, J.C.; Cottrell, S.J.; Feeder, N.; Galek, P.T.A.; Groom, C.R.; Pidcock, E. Evaluation of molecular crystal structures using Full Interaction Maps. *CrystEngComm* **2013**, *15*, 65–72. [CrossRef]
246. Golovanov, A.A.; Latypova, D.R.; Bekin, V.V.; Pisareva, V.S.; Vologzhanina, A.V.; Dokichev, V.A. Synthesis of 1,5-disubstituted (E)-pent-2-en-4-yn-1-ones. *Russ. J. Org. Chem.* **2013**, *49*, 1264–1269. [CrossRef]
247. Vologzhanina, A.V.; Golovanov, A.A.; Gusev, D.M.; Odin, I.S.; Apreyan, R.A.; Suponitsky, K.Yu. Intermolecular Interactions and Second-Harmonic Generation Properties of (E)-1,5-Diarylpentenyn-1-ones. *Cryst. Growth Des.* **2014**, *14*, 4402–4410. [CrossRef]
248. Mugheirbi, N.A.; Tajber, L. Crystal Habits of Itraconazole Microcrystals: Unusual Isomorphic Intergrowths Induced via Tuning Recrystallization Conditions. *Mol. Pharm.* **2015**, *12*, 3468–3478. [CrossRef] [PubMed]
249. Sandhu, B.; Sinha, A.S.; Desper, J.; Aakeröy, C.B. Modulating the physical properties of solid forms of urea using co-crystallization technology. *Chem. Commun.* **2018**, *54*, 4657–4660. [CrossRef] [PubMed]
250. Wojnarska, J.; Gryl, M.; Seidler, T.; Stadnicka, K.M. Crystal engineering, optical properties and electron density distribution of polar multicomponent materials containing sulfanilamide. *CrystEngComm* **2018**, *20*, 3638–3646. [CrossRef]
251. Xing, G.; Bassanetti, I.; Ben, T.; Bracco, S.; Sozzani, P.; Marchiò, L.; Comotti, A. Multifunctional Organosulfonate Anions Self-Assembled with Organic Cations by Charge-Assisted Hydrogen Bonds and the Cooperation of Water. *Cryst. Growth Des.* **2018**, *18*, 2082–2092. [CrossRef]
252. Honorato, J.; Colina-Vegas, L.; Correa, R.S.; Guedes, A.P.M.; Miyata, M.; Pavan, F.R.; Ellena, J.; Batista, A.A. Esterification of the free carboxylic group from the lutidinic acid ligand as a tool to improve the cytotoxicity of Ru(II) complexes. *Inorg. Chem. Front.* **2019**, *6*, 376–390. [CrossRef]
253. Kodrin, I.; Soldin, Ž.; Aakeröy, C.B.; Đaković, M. Role of the "Weakest Link" in a Pressure-Driven Phase Transition of Two Polytypic Polymorphs. *Cryst. Growth Des.* **2016**, *16*, 2040–2051. [CrossRef]
254. Moggach, S.A.; Marshall, W.G.; Rogers, D.M.; Parsons, S. How focussing on hydrogen bonding interactions in amino acids can miss the bigger picture: A high-pressure neutron powder diffraction study of ε-glycine. *CrystEngComm* **2015**, *17*, 5315–5328. [CrossRef]

255. Voronova, E.D.; Golovanov, A.A.; Suponitsky, K.Yu.; Fedyanin, I.V.; Vologzhanina, A.V. Theoretical Charge Density Analysis and Nonlinear Optical Properties of Quasi-Planar 1-Aryl(hetaryl)-5-phenylpent-1-en-4-yn-3-ones. *Cryst. Growth Des.* **2016**, *16*, 3859–3868. [CrossRef]
256. Vráblová, A.; Černák, J.; Falvello, L.R.; Tomás, M. Polymorphism of the dinuclear $Co^{III}$–Schiff base complex $[Co^2(o\text{-van-en})^3]\cdot 4CH^3CN$ (o-van-en is a salen-type ligand). *Acta Cryst. Sect. C* **2019**, *75*, 433–442. [CrossRef]
257. Voronova, E.D.; Golovanov, A.A.; Odin, I.S.; Anisimov, M.A.; Dorovatovskii, P.V.; Zubavichus, Y.V.; Vologzhanina, A.V. Peculiarities of supramolecular organization of cyclic ketones with vinylacetylene fragments. *Acta Cryst. Sect. C* **2018**, *74*, 1674–1683. [CrossRef]
258. Dotsenko, V.V.; Frolov, K.A.; Krivokolysko, S.G.; Chigorina, E.A.; Pekhtereva, T.M.; Suykov, S.Yu.; Papayanina, E.S.; Dmitrienko, A.O.; Bushmarinov, I.S. Aminomethylation of morpholinium and N-methylmorpholinium 3,5-dicyano-4,4-dimethyl-6-oxo-1,4,5,6-tetrahydropyridine-2-thiolates. *Chem. Heterocycl. Comp.* **2016**, *52*, 116–127. [CrossRef]
259. Carletta, A.; Zbačnik, M.; Van Gysel, M.; Vitković, M.; Tumanov, N.; Stilinović, V.; Wouters, J.; Cinčić, D. Playing with Isomerism: Cocrystallization of Isomeric N-Salicylideneaminopyridines with Perfluorinated Compounds as Halogen Bond Donors and Its Impact on Photochromism. *Cryst. Growth Des.* **2018**, *18*, 6833–6842. [CrossRef]
260. Mugheirbi, N.A.; Tajber, L. Mesophase and size manipulation of itraconazole liquid crystalline nanoparticles produced via quasi nanoemulsion precipitation. *Eur. J. Pharm. Biopharm.* **2015**, *96*, 226–236. [CrossRef] [PubMed]
261. Cole, J.C.; Kabova, E.A.; Shankland, K. Utilizing organic and organometallic structural data in powder diffraction. *Powder Diffr.* **2014**, *29*, S19–S30. [CrossRef]
262. Anisimov, A.A.; Zhemchugov, P.V.; Milenin, S.A.; Goloveshkin, A.S.; Tsareva, U.S.; Bushmarinov, I.S.; Korlyukov, A.A.; Takazova, R.U.; Molodtsova, Y.A.; Muzafarov, A.M.; et al. Sodium cis-tetratolylcyclotetrasiloxanolate and cis-tritolylcyclotrisiloxanolate: Synthesis, structure and their mutual transformations. *J. Organomet. Chem.* **2016**, *823*, 103–111. [CrossRef]
263. Taylor, R.; Cole, J.; Korb, O.; McCabe, P. Knowledge-Based Libraries for Predicting the Geometric Preferences of Druglike Molecules. *J. Chem. Inf. Model.* **2014**, *54*, 2500–2514. [CrossRef] [PubMed]
264. Cole, J.C.; Korb, O.; McCabe, P.; Read, M.G.; Taylor, R. Knowledge-Based Conformer Generation Using the Cambridge Structural Database. *J. Chem. Inf. Model.* **2018**, *58*, 615–629. [CrossRef] [PubMed]
265. Giangreco, I.; Olsson, T.S.G.; Cole, J.C.; Packer, M.J. Assessment of a Cambridge Structural Database-Driven Overlay Program. *J. Chem. Inf. Model.* **2014**, *54*, 3091–3098. [CrossRef] [PubMed]
266. Capucci, D.; Balestri, D.; Mazzeo, P.P.; Pelagatti, P.; Rubini, K.; Bacchi, A. Liquid Nicotine Tamed in Solid Forms by Cocrystallization. *Cryst. Growth Des.* **2017**, *17*, 4958–4964. [CrossRef]
267. Habgood, M. Bioactive focus in conformational ensembles: A pluralistic approach. *J. Comput. Aided Mol. Des.* **2017**, *31*, 1073–1083. [CrossRef] [PubMed]
268. Iuzzolino, L.; Reilly, A.M.; McCabe, P.; Price, S.L. Use of Crystal Structure Informatics for Defining the Conformational Space Needed for Predicting Crystal Structures of Pharmaceutical Molecules. *J. Chem. Theory Comput.* **2017**, *13*, 5163–5171. [CrossRef]
269. Iuzzolino, L.; McCabe, P.; Price, S.L.; Brandenburg, J.G. Crystal structure prediction of flexible pharmaceutical-like molecules: Density functional tight-binding as an intermediate optimisation method and for free energy estimation. *Faraday Discuss.* **2018**, *211*, 275–296. [CrossRef] [PubMed]
270. Pal, S.K.; Zewail, A.H. Dynamics of Water in Biological Recognition. *Chem. Rev.* **2004**, *104*, 2099–2124. [CrossRef]
271. Terao, H.; Sugawara, T.; Kita, Y.; Sato, N.; Kaho, E.; Takeda, S. Proton Relay in a One-Dimensional Hydrogen-Bonded Chain Composed of Water Molecules and a Squaric Acid Derivative. *J. Am. Chem. Soc.* **2001**, *123*, 10468–10474. [CrossRef] [PubMed]
272. Ananyev, I.V.; Bushmarinov, I.S.; Ushakov, I.E.; Aitkulova, A.I.; Lyssenko, K.A. Tuning of the double-well potential of short strong hydrogen bonds by ionic interactions in alkali metal hydrodicarboxylates. *RSC Adv.* **2015**, *5*, 97495–97502. [CrossRef]
273. Hickey, M.B.; Peterson, M.L.; Manas, E.S.; Alvarez, J.; Haeffner, F.; Almarsson, Ö. Hydrates and Solid-State Reactivity: A Survey of β-Lactam Antibiotics. *J. Pharm. Sci.* **2007**, *96*, 1090–1099. [CrossRef]

274. Xu, H.-R.; Zhang, Q.-C.; Ren, Y.-P.; Zhao, H.-X.; Long, L.-S.; Huang, R.-B.; Zheng, L.-S. The influence of water on dielectric property in cocrystal compound of [orotic acid] [melamine]·$H_2O$. *CrystEngComm* **2011**, *13*, 6361–6364. [CrossRef]
275. Ananyev, I.V.; Barzilovich, P.Yu.; Lyssenko, K.A. Evidence for the Zundel-like Character of Oxoethylidenediphosphonic Acid Hydrate. *Mendeleev Commun.* **2012**, *22*, 242–244. [CrossRef]
276. Liu, F.; Hooks, D.E.; Li, N.; Mara, N.A.; Swift, J.A. Mechanical Properties of Anhydrous and Hydrated Uric Acid Crystals. *Chem. Mater.* **2018**, *30*, 3798–3805. [CrossRef]
277. Silverstein, K.A.T.; Haymet, A.D.J.; Dill, K.A. A Simple Model of Water and the Hydrophobic Effect. *J. Am. Chem. Soc.* **1998**, *120*, 3166–3175. [CrossRef]
278. Ludwig, R. Water: From Clusters to the Bulk. *Angew. Chem. Int. Ed.* **2001**, *40*, 1808–1827. [CrossRef]
279. Takeuchi, F.; Hiratsuka, M.; Ohmura, R.; Alavi, S.; Sum, A.K.; Yasuoka, K. Water proton configurations in structures I, II, and H clathrate hydrate unit cells. *J. Chem. Phys.* **2013**, *138*, 124504. [CrossRef] [PubMed]
280. Joseph, A.; Alves, J.S.R.; Bernardes, C.E.S.; Piedade, M.F.M.; Piedade, M.E.M. da Tautomer selection through solvate formation: The case of 5-hydroxynicotinic acid. *CrystEngComm* **2019**, *21*, 2220–2233. [CrossRef]
281. Medvedev, A.G.; Mikhailov, A.A.; Prikhodchenko, P.V.; Tripol'skaya, T.A.; Lev, O.; Churakov, A.V. Crystal structures of pyridinemonocarboxylic acid peroxosolvates. *Russ. Chem. Bull.* **2013**, *62*, 1871–1876. [CrossRef]
282. Gillon, A.L.; Feeder, N.; Davey, R.J.; Storey, R. Hydration in Molecular Crystals. A Cambridge Structural Database Analysis. *Cryst. Growth Des.* **2003**, *3*, 663–673. [CrossRef]
283. Puntus, L.N.; Lyssenko, K.A.; Pekareva, I.S.; Bünzli, J.-C.G. Intermolecular Interactions as Actors in Energy-Transfer Processes in Lanthanide Complexes with 2,2'-Bipyridine. *J. Phys. Chem. B* **2009**, *113*, 9265–9277. [CrossRef]
284. Nelyubina, Y.V.; Puntus, L.N.; Lyssenko, K.A. The Dark Side of Hydrogen Bonds in the Design of Optical Materials: A Charge-Density Perspective. *Chem. Eur. J.* **2014**, *20*, 2860–2865. [CrossRef]
285. Banaru, A.M.; Slovokhotov, Y.L. Crystal hydrates of organic compounds. *J. Struct. Chem.* **2015**, *56*, 967–982. [CrossRef]
286. Dobrzycki, Ł.; Socha, P.; Ciesielski, A.; Boese, R.; Cyrański, M.K. Formation of Crystalline Hydrates by Nonionic Chaotropes and Kosmotropes: Case of Piperidine. *Cryst. Growth Des.* **2019**, *19*, 1005–1020. [CrossRef]
287. Siddiqui, K.A. Structural Diversity of Metal–organic Hydrates: A Crystallographic Structural Database Study. *J Struct. Chem.* **2018**, *59*, 106–113. [CrossRef]
288. Infantes, L.; Fábián, L.; Motherwell, W.D.S. Organic crystal hydrates: What are the important factors for formation. *CrystEngComm* **2007**, *9*, 65–71. [CrossRef]
289. Desiraju, G.R. Hydration in organic crystals: Prediction from molecular structure. *J. Chem. Soc. Chem. Commun.* **1991**, 426–428. [CrossRef]
290. Van de Streek, J.; Motherwell, S. New software for searching the Cambridge Structural Database for solvated and unsolvated crystal structures applied to hydrates. *CrystEngComm* **2007**, *9*, 55–64. [CrossRef]
291. Bajpai, A.; Scott, H.S.; Pham, T.; Chen, K.-J.; Space, B.; Lusi, M.; Perry, M.L.; Zaworotko, M.J. Towards an understanding of the propensity for crystalline hydrate formation by molecular compounds. *IUCrJ* **2016**, *3*, 430–439. [CrossRef] [PubMed]
292. Brychczynska, M.; Davey, R.J.; Pidcock, E. A study of methanol solvates using the Cambridge structural database. *New J. Chem.* **2008**, *32*, 1754–1760. [CrossRef]
293. Brychczynska, M.; Davey, R.J.; Pidcock, E. A study of dimethylsulfoxide solvates using the Cambridge Structural Database (CSD). *CrystEngComm* **2012**, *14*, 1479–1484. [CrossRef]
294. Spiteri, L.; Baisch, U.; Vella-Zarb, L. Correlations and statistical analysis of solvent molecule hydrogen bonding—a case study of dimethyl sulfoxide (DMSO). *CrystEngComm* **2018**, *20*, 1291–1303. [CrossRef]
295. Navasardyan, M.A.; Grishanov, D.A.; Tripol'skaya, T.A.; Kuz'mina, L.G.; Prikhodchenko, P.V.; Churakov, A.V. Crystal structures of non-proteinogenic amino acid peroxosolvates: Rare example of H-bonded hydrogen peroxide chains. *CrystEngComm* **2018**, *20*, 7413–7416. [CrossRef]
296. Inokuma, Y.; Matsumura, K.; Yoshioka, S.; Fujita, M. Finding a New Crystalline Sponge from a Crystallographic Database. *Chem.—Asian J.* **2017**, *12*, 208–211. [CrossRef]
297. Byrn, S.R.; Lin, C.-T. The effect of crystal packing and defects on desolvation of hydrate crystals of caffeine and L-(-)-1,4-cyclohexadiene-1-alanine. *J. Am. Chem. Soc.* **1976**, *98*, 4004–4005. [CrossRef]

298. Leung, S.S.; Padden, B.E.; Munson, E.J.; Grant, D.J.W. Hydration and Dehydration Behavior of Aspartame Hemihydrate. *J. Pharm. Sci.* **1998**, *87*, 508–513. [CrossRef] [PubMed]
299. Saha, R.; Biswas, S.; Steele, I.M.; Dey, K.; Jana, A.D.; Kumar, S. Stabilization of 2D water sheets in a supramolecular metal–organic Schiff base complex: Reversible structural transformation upon dehydration–rehydration. *Inorg. Chim. Acta* **2013**, *399*, 200–207. [CrossRef]
300. Zhang, H.; Yin, Z. Discrete cage form of water hexamer in the hydrophilic channels assembled by heterocyclic azopyrrole. *J. Mol. Struct.* **2015**, *1092*, 9–13. [CrossRef]
301. Vologzhanina, A.V.; Zorina-Tikhonova, E.N.; Matyukhina, A.K.; Sidorov, A.A.; Dorovatovskii, P.V.; Eremenko, I.L. 36-Nuclear anionic cobalt(II) and nickel(II) complexes in solid-phase insertion reactions. *Russ. J. Coord. Chem.* **2017**, *43*, 801–806. [CrossRef]
302. Willart, J.F.; Danede, F.; De Gusseme, A.; Descamps, M.; Neves, C. Origin of the Dual Structural Transformation of Trehalose Dihydrate upon Dehydration. *J. Phys. Chem. B* **2003**, *107*, 11158–11162. [CrossRef]
303. Gillon, A.L.; Davey, R.J.; Storey, R.; Feeder, N.; Nichols, G.; Dent, G.; Apperley, D.C. Solid State Dehydration Processes: Mechanism of Water Loss from Crystalline Inosine Dihydrate. *J. Phys. Chem. B* **2005**, *109*, 5341–5347. [CrossRef] [PubMed]
304. Fucke, K.; Steed, J.W. X-ray and Neutron Diffraction in the Study of Organic Crystalline Hydrates. *Water* **2010**, *2*, 333–350. [CrossRef]
305. Braun, D.E.; Griesser, U.J. Supramolecular Organization of Nonstoichiometric Drug Hydrates: Dapsone. *Front. Chem.* **2018**, *6*, 31. [CrossRef] [PubMed]
306. Białońska, A.; Ciunik, Z.; Ilczyszyn, M.M.; Siczek, M. Discrete Cuboidal 15- and 16-Membered Water Clusters in Brucine 3.86-Hydrate, Water Release and Its Consequences. *Cryst. Growth Des.* **2014**, *14*, 6537–6541. [CrossRef]
307. Febles, M.; Pérez-Hernández, N.; Pérez, C.; Rodríguez, M.L.; Foces-Foces, C.; Roux, M.V.; Morales, E.Q.; Buntkowsky, G.; Limbach, H.-H.; Martín, J.D. Distinct Dynamic Behaviors of Water Molecules in Hydrated Pores. *J. Am. Chem. Soc.* **2006**, *128*, 10008–10009. [CrossRef]
308. CSD Python API Forum. Available online: https://www.ccdc.cam.ac.uk/forum/csd_python_api (accessed on 14 August 2019).
309. Moghadam, P.Z.; Li, A.; Wiggin, S.B.; Tao, A.; Maloney, A.G.P.; Wood, P.A.; Ward, S.C.; Fairen-Jimenez, D. Development of a Cambridge Structural Database Subset: A Collection of Metal–Organic Frameworks for Past, Present, and Future. *Chem. Mater.* **2017**, *29*, 2618–2625. [CrossRef]
310. Dolinar, B.S.; Samedov, K.; Maloney, A.G.P.; West, R.; Khrustalev, V.N.; Guzei, I.A. A chiral diamine: Practical implications of a three-stereoisomer cocrystallization. *Acta Cryst. Sect. C* **2018**, *74*, 54–61. [CrossRef] [PubMed]
311. Bryant, M.J.; Maloney, A.G.P.; Sykes, R.A. Predicting mechanical properties of crystalline materials through topological analysis. *CrystEngComm* **2018**, *20*, 2698–2704. [CrossRef]
312. Miklitz, M.; Jelfs, K.E. pywindow: Automated Structural Analysis of Molecular Pores. *J. Chem. Inf. Model.* **2018**, *58*, 2387–2391. [CrossRef] [PubMed]
313. Park, S.; Kim, B.; Choi, S.; Boyd, P.G.; Smit, B.; Kim, J. Text Mining Metal–Organic Framework Papers. *J. Chem. Inf. Model.* **2018**, *58*, 244–251. [CrossRef] [PubMed]
314. Hussain, J.; Rea, C. Computationally Efficient Algorithm to Identify Matched Molecular Pairs (MMPs) in Large Data Sets. *J. Chem. Inf. Model.* **2010**, *50*, 339–348. [CrossRef] [PubMed]
315. Zolotarev, P.N.; Arshad, M.N.; Asiri, A.M.; Al-amshany, Z.M.; Blatov, V.A. A Possible Route toward Expert Systems in Supramolecular Chemistry: 2-Periodic H-Bond Patterns in Molecular Crystals. *Cryst. Growth Des.* **2014**, *14*, 1938–1949. [CrossRef]
316. Blatova, O.A.; Asiri, A.M.; Al-amshany, Z.M.; Arshad, M.N.; Blatov, V.A. Molecular packings and specific-bonding patterns in sulfonamides. *New J. Chem.* **2014**, *38*, 4099–4106. [CrossRef]
317. Baburin, I.A.; Blatov, V.A.; Carlucci, L.; Ciani, G.; Proserpio, D.M. Interpenetrated Three-Dimensional Networks of Hydrogen-Bonded Organic Species: A Systematic Analysis of the Cambridge Structural Database. *Cryst. Growth Des.* **2008**, *8*, 519–539. [CrossRef]
318. Klamt, A. Conductor-like Screening Model for Real Solvents: A New Approach to the Quantitative Calculation of Solvation Phenomena. *J. Phys. Chem.* **1995**, *99*, 2224–2235. [CrossRef]
319. Klamt, A.; Jonas, V.; Bürger, T.; Lohrenz, J.C.W. Refinement and Parametrization of COSMO-RS. *J. Phys. Chem. A* **1998**, *102*, 5074–5085. [CrossRef]

320. Tilbury, C.J.; Chen, J.; Mattei, A.; Chen, S.; Sheikh, A.Y. Combining Theoretical and Data-Driven Approaches To Predict Drug Substance Hydrate Formation. *Cryst. Growth Des.* **2018**, *18*, 57–67. [CrossRef]
321. *Chem3D*, version 18.2 Suite; Perkin Elmer Corporation: Waltham, MA, USA, 2016.
322. CCDC Documentation and Resources. Available online: https://ccdc.cam.ac.uk/support-and-resources/ccdcresources/ (accessed on 14 August 2019).